Emergent competition resolves the paradox of stable microbial mutualisms

Oliver J. Meacock *[1,2], Massimo Amicone [2], and Sara Mitri [2]

[1]School of Biosciences, University of Sheffield, Sheffield, United Kingdom

[2]Department of Fundamental Microbiology, University of Lausanne, Lausanne, Switzerland

Abstract

What is the role of cooperation in determining ecosystem structure? This question is central to ecology, yet remains controversial; cooperative mechanisms such as plant-insect pollination and microbe-microbe cross-feeding are widespread, but ecological theory suggests that cooperative communities should be unstable. Here, we resolve this apparent contradiction by deriving a precise and general mapping between mechanistic interaction models and the generalised Lotka-Volterra (gLV) equation. By avoiding the common assumption that environmental and population dynamics occur on different timescales, we obtain a framework that is built on the rate of change of growth rates, *i.e.* growth accelerations. We apply our findings to a model of an obligatory mutualism between auxotrophic bacteria and obtain a counter-intuitive result: increasing the strength of cooperative mechanisms by increasing amino acid production rates causes competition over shared resources to become stronger. At the same time, effective intrinsic growth rates become increasingly positive. These coupled effects allow enhanced cross-feeding to increase overall population sizes while maintaining ecosystem stability. Finally, we exploit an exact correspondence between mechanistic models and Modern Coexistence Theory (MCT) to provide mechanistic insights into resulting coexistence outcomes and predict coexistence in experimental gut communities. Our findings show that cooperative and competitive interaction mechanisms do not necessarily translate into positive and negative interaction strengths in phenomenological models, highlighting the importance of mechanistic insights for developing a correct understanding of ecosystem structure.

*o.meacock@sheffield.ac.uk

1 Introduction

Mutually-beneficial interactions between populations, or mutualisms, are key to the establishment and persistence of organisms in ecosystems across scales [1]. While originally studied in the context of relationships between macroscopic organisms such as plants and their pollinators or cleaner fish and their clients, mutualistic relationships are now known to be fundamental to the composition of many microbial ecosystems [2]. In the most extreme cases, isolates initially identified as pure cultures of single species have been unmasked as assemblies of mutually-dependent bacteria upon closer examination [3, 4]. More broadly, auxotrophic microbes that lack the ability to synthesise essential vitamins, amino acids and/or neucleotides are widespread in the environment and human-associated microbiomes [5–7]. Such metabolic deficiencies must be compensated for by secretions from surrounding organisms to allow auxotrophic species to persist. The diversity and function of microbiomes is thus strongly influenced by nutritional exchanges [2, 8, 9].

Surprisingly, despite these widespread observations of mutualisms in nature, theoretical investigations based on the generalised Lotka-Volterra (gLV) framework and related models suggest that mutualisms should destabilise ecosystems [10–12]. Reconciling these apparently contradictory results has been a pressing challenge for theoretical ecologists in recent decades [13–18]. While introducing more realistic representations of the underlying biological processes mediating interactions can enhance the stability of mutualisms [19–22] , these modifications remain largely *ad hoc* as they are not derived from an explicit mechanistic representation of the system. Instead, they are based on intuitive but untested assumptions of how changes to interaction mechanisms should impact interaction values.

There is a fundamental technical barrier to resolving this problem using theory: while we can explicitly represent the mechanisms that mediate mutualisms (*e.g.* nutritional exchanges [23–25]) relatively straightforwardly, we have thus far been unable to identify a generic mapping between these mechanistic models and phenomenological interaction frameworks such as the gLV model. Achieving such a mapping is a long sought-after goal in theoretical ecology, first attempted by MacArthur in his pioneering work on resource competition [26]. However, despite decades of efforts to understand the connections between these two frameworks [25, 27–31], a general formulation for identifying equivalencies between the two remains elusive. Several studies have highlighted fundamental differences between their predictions and structures,

suggesting that a direct correspondence may not exist [32–34].

In this work, we resolve this challenge by deriving a general and precise mapping between mechanistic and phenomenological interaction frameworks that is based on growth accelerations rather than rates. Conveniently, our results allow us to directly apply much of the theoretical toolset built to study the gLV equation to mechanistic interaction models. By applying these tools to a two-population model of cross-feeding auxotrophic bacteria, we show that manipulating mechanistic parameters can result in counter-intuitive effects on effective gLV parameters. Specifically, we show that increasing the production rate of cross-fed compounds paradoxically increases effective competition between mutualists. This effect emerges because cross-fed nutrients become less growth limiting as their production is increased. Consequently, growth limitation imposed by non cross-fed resources that are consumed by both mutualists becomes more dominant. Changes in coexistence outcomes resulting from these mechanistic changes can be exactly captured by applying Modern Coexistence Theory (MCT) through our framework, with stronger cross-feeding exchanges increasing niche overlap. Our findings thus provide an unexpected explanation for the stability of microbial mutualisms that is rooted in an understanding of interaction mechanisms.

2 Results

2.1 A generic mapping between mechanistic and phenomenological interaction frameworks

In phenomenological frameworks such as the gLV model, growth rates are shaped purely by population densities (Fig. 1a). The gLV model assumes a linear impact of partner density on a focal populations' per-capita growth rate (PCGR, defined as $\frac{1}{x_\alpha}\frac{dx_\alpha}{dt}$):

$$\frac{1}{x_\alpha}\frac{dx_\alpha}{dt} = \mu_\alpha + \sum_\beta a_{\alpha\beta}x_\beta. \tag{1}$$

Here, x_α is the instantaneous density of focal population α, μ_α is the 'intrinsic growth rate' of α (its growth rate at low densities and in the absence of other populations) and $a_{\alpha\beta}$ are the interaction strengths (the growth rate impact of one unit of population β on α). These can be assembled into an interaction matrix A [35].

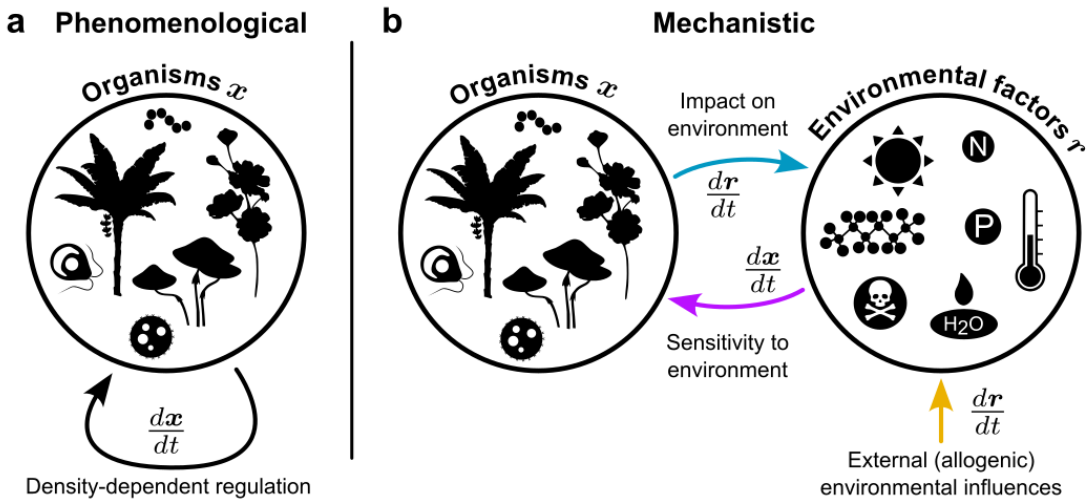

Figure 1: **Structures of phenomenological and mechanistic ecosystem models.** Colours of arrows in panel b correspond to the colour scheme used throughout this manuscript for impact functions (blue), sensitivity functions (purple) and allogenic functions (gold).

Alternatively, interaction mechanisms can be explicitly represented by splitting the ecosystem into two groups of dynamical quantities: the sizes of the populations of interest $\boldsymbol{x}$ and the quantities of environmental factors $\boldsymbol{r}$ that influence these populations' growth rates (Fig. 1b). Although often treated as the concentrations of abiotic environmental compounds in plant and microbial community ecology [36, 37], these are more general and may also include factors such as biotic resources that can self-replicate [26]. The key structural determinant of these models is that they are bipartite: $\boldsymbol{x}$ can influence $\boldsymbol{r}$ and $\boldsymbol{r}$ can influence $\boldsymbol{x}$, but there are no direct relationships between different members of $\boldsymbol{x}$ or $\boldsymbol{r}$.

The dynamics of the environmental factors are determined by a combination of impacts by the community, which we represent with environment-dependent impact functions $\boldsymbol{f}_\beta(\boldsymbol{r})$ [31], and extrinsic processes that are independent of the community (*e.g.* fluxes of compounds into the ecosystem or reproduction of biotic resources) which we represent with the allogenic function $\boldsymbol{\sigma}(\boldsymbol{r})$. Putting these together, we can then write the rate of change of the environmental factors $\boldsymbol{r}$ as:

$$\frac{d\boldsymbol{r}}{dt} = \sum_\beta x_\beta \boldsymbol{f}_\beta(\boldsymbol{r}) + \boldsymbol{\sigma}(\boldsymbol{r}) \tag{2}$$

The *sensitivity function* g_α describes the growth rate of a population α in a particular environment:

$$\frac{1}{x_\alpha}\frac{dx_\alpha}{dt} = g_\alpha(\boldsymbol{r}). \tag{3}$$

While these are often described as the basic equations of consumer-resource models [38], we refer to this class of system more generally as Environment-Organism (EO) models to emphasise that environmental factors need not be resources and that population need not consume them [37, 39]. The impact and sensitivity functions together encode the mechanisms through which the populations x interact, and can be constructed to describe a very broad range of biological processes [18, 36] (Table S1).

Identifying a general way to convert these expressions into a gLV-like equation (Eq. 1) is desirable as it would allow us to understand how underlying interaction mechanisms ultimately shape coexistence. Current techniques for performing this mapping rely on approximations such as the separation of timescales between environmental and population dynamics [25, 26, 31, 40] or low population densities [30], or are applicable only to specially-selected EO systems with convenient algebraic properties [27, 28, 36]. A common feature of most such approaches is their adoption of a first order perspective, aiming to derive an expression that describes growth rates in terms of the population densities as in the gLV equation. However, interactions in mechanistic models result from the combination of two rate-based processes [41, 42]: the rate at which organisms impact the environment and the sensitivity of their growth rates to environmental conditions. The combination of two first order processes might be expected to lead to second order dynamics, *i.e.* growth accelerations.

Following this logic, we can evaluate the temporal derivative of the populations' PCGRs to obtain the per-capita growth acceleration (PCGA, $\frac{d}{dt}\left(\frac{1}{x_\alpha}\frac{dx_\alpha}{dt}\right)$):

$$\frac{d}{dt}\left(\frac{1}{x_\alpha}\frac{dx_\alpha}{dt}\right) = \nabla g_\alpha \cdot \frac{d\boldsymbol{r}}{dt}, \tag{4}$$

where we have used the multivariable chain rule to split the temporal derivative of the sensitivity function into the sensitivity gradients with respect to the environmental factors ($\nabla g_\alpha \equiv \frac{\partial g_\alpha}{\partial \boldsymbol{r}}$) and the rate of environmental change. Substituting in Eq. 2, we obtain (Supplementary Note 1.1):

$$\frac{d}{dt}\left(\frac{1}{x_\alpha}\frac{dx_\alpha}{dt}\right) = \mu'_\alpha(\boldsymbol{r}) + \sum_\beta a'_{\alpha\beta}(\boldsymbol{r})x_\beta. \tag{5}$$

This equation, which we will refer to as the accelerational Environment-Organism (aEO) equation, partitions the PCGA into two parts: the abiotic acceleration $\mu'_\alpha(\boldsymbol{r}) \equiv \boldsymbol{\sigma}(\boldsymbol{r}) \cdot \nabla g_\alpha(\boldsymbol{r})$ represents the rate of change of the growth rate of α due to the extrinsic drivers of the environmental factors, while the term $\sum_\beta a'_{\alpha\beta}(\boldsymbol{r})x_\beta$ captures the growth rate impacts caused by the community's impact on the environmental factors. Central to this term are the biotic accelerations $a'_{\alpha\beta}(\boldsymbol{r}) \equiv \boldsymbol{f}_\beta(\boldsymbol{r}) \cdot \nabla g_\alpha(\boldsymbol{r})$, which capture the per-capita contribution to this effect from each community member.

Despite the fact that the gLV equation is first order and the aEO equation is second order, there are deep equivalencies between the two. Notably, at an equilibrium state in environment $\boldsymbol{r}^*$, $\frac{d}{dt}\left(\frac{1}{x_\alpha}\frac{dx_\alpha}{dt}\right) = 0$. We therefore obtain

$$0 = \mu'_\alpha(\boldsymbol{r}^*) + \sum_\beta a'_{\alpha\beta}(\boldsymbol{r}^*)x_\beta, \tag{6}$$

i.e. an expression that is algebraically identical to the gLV equation (Eq. 1) at equilibrium. This result means that for many rate-based mathematical statements which are true for an equilibrium gLV system, there is a parallel acceleration-based statement which holds for all equilibrium EO systems. We discuss some of the tools that can be built through this parallelism in Supplementary Note 1.3. This result is exact and general, only requiring that $g_\alpha(\boldsymbol{r})$ is smooth with respect to the environmental factors, such that the sensitivity gradient $\nabla g_\alpha(\boldsymbol{r})$ is well-defined.

2.2 A simulated cross-feeding community demonstrates counter-intuitive relationships between interaction mechanisms and effective gLV parameters

To illustrate how these results inform our understanding of mutualistic exchanges in microbial ecosystems, we built a two-population EO model representing obligate cross-feeding between two auxotrophic bacterial populations, $\mathring{v}$ and $\mathring{w}$, which must be fed with amino acids v and w respectively. This type of system is a popular choice for studying mutualisms in the lab [24, 43–47]

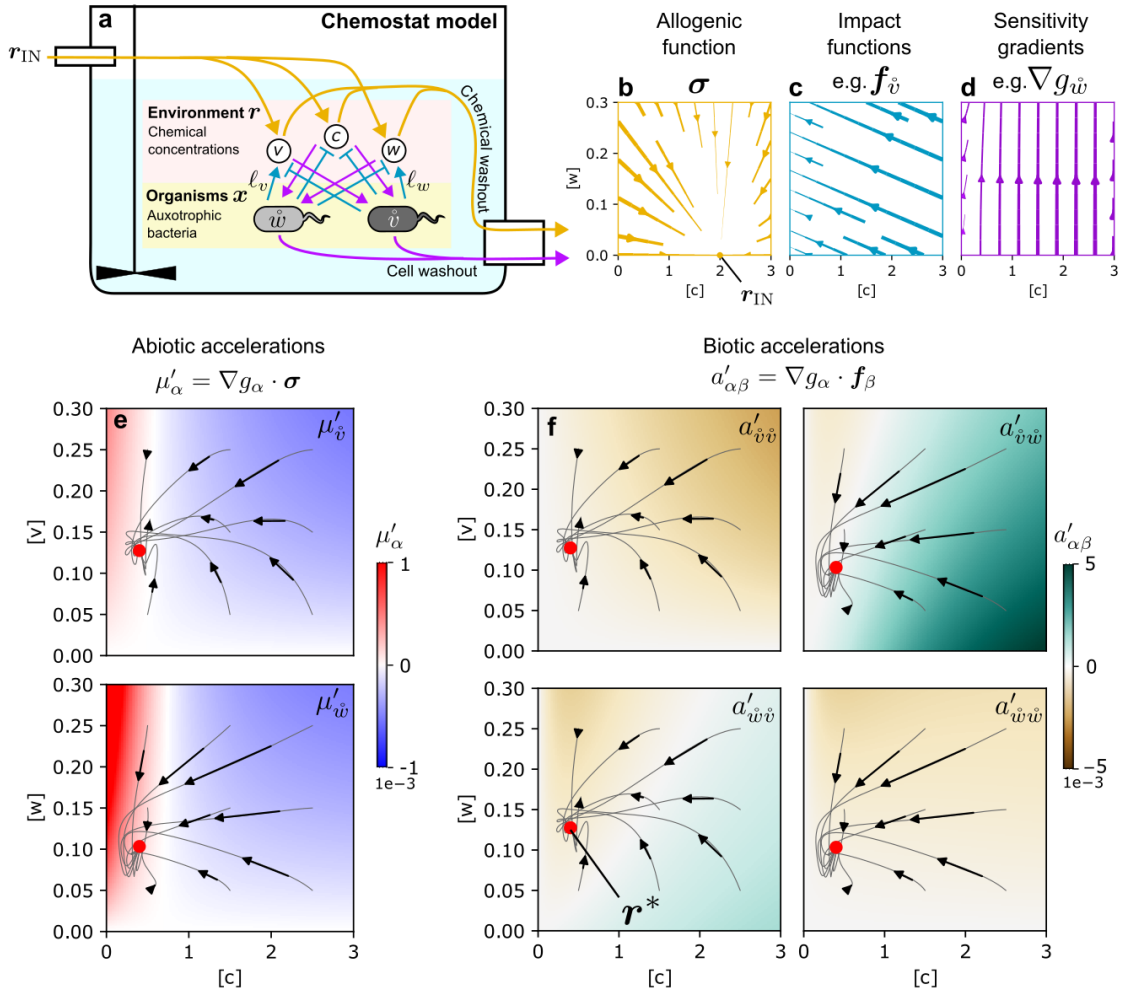

Figure 2: **An accelerational description of cross-feeding auxotrophs at equilibrium.** EO models consist of three components – allogenic functions, sensitivities and impacts - that together represent the mechanisms through which organisms interact. a) We built an EO model representing a community of two cross-feeding auxotrophic bacteria (each unable to synthesise one of two amino acids v and w) in a chemostat. Metabolic dependencies on a carbon source c and amino acids are encoded by sensitivity functions (purple), while consumption and production are represented by impact functions (blue, arrows indicate production, bars consumption). These functions are constructed using explicit mechanistic parameters such as the amino acid production rates ℓ_v and ℓ_w. Allogenic processes in this system (gold) are the external influences on chemical concentrations, *i.e.* nutrient influx and washout of chemicals through the chemostat efflux. Washout of cells at the same rate also acts as an effective mortality term. b-d) These three processes can be represented as vector fields in the 'environment space', the space of possible environmental compositions r. e,f) Taking the scalar product of the sensitivity gradients and allogenic function yields the abiotic accelerations (e), while the scalar product of the sensitivity gradients and impact functions yields the biotic accelerations (f). These can be represented as scalar fields sitting in the environment space. The chemical environment converges on an equilibrium composition r^* (red circle) regardless of the starting composition of the media in the chemostat (grey trajectories and arrows). Note that the full environment space is three dimensional, representing the concentrations of c, v and w (Fig. S2). In b-f, we display slices through this space for which the concentration of the chemical corresponding to the suppressed axis is set to zero. Environmental trajectories (e,f) are projected onto this plane. Arrow thickness in b-d indicates the local magnitude of the vector field. Dilution rate $D = 0.01$.

and is widely observed in environmental microbiomes [2, 4, 6]. Our formulation (Methods, Table S2) assumes that growth depends on co-utilisation of a carbon source c (used by both partners) and a population-specific amino acid (v or w) that is secreted by the mutualistic partner. We also include 'overflow' production of amino acids when an auxotroph's essential amino acid is at low concentrations but the concentration of the carbon source is high, reflecting recent experimental findings [48] (Fig. 2a). This community was then placed into a simulated chemostat, an idealised representation of systems with continual inflows and outflows of material such as the gut [49]. In the absence of external amnio acids, this model has multiple features of obligatory mutualisms including bistability and Allee effects [21] (Fig. S1).

The mechanistic processes that define an EO model can be represented as vector fields sitting in the 'environment space', which represents all possible combinations of the environmental factors (Figs. 2b-d, S2). The allogenic function and impact functions indicate the direction that the environment is pulled by the abiotic and biotic influences on the environment, respectively. For example, dilution of a chemostat's content with media of composition $\boldsymbol{r}_{\text{IN}}$ results in an allogenic function in which all vectors point towards $\boldsymbol{r}_{\text{IN}}$ (Fig. 2b). Sensitivity gradients can also be represented as vector fields, now representing the rate at which a population's growth rate changes as the environment is pulled in a given direction (Fig. 2d). Taking scalar products of these vector fields give scalar fields that represent the rate at which the growth rate of population α is modified by the external drivers of the environmental dynamics (the abiotic acceleration, $\mu'_\alpha(\boldsymbol{r})$) or by the effect of another community member β on the environment (the biotic accelerations, $a'_{\alpha\beta}(\boldsymbol{r})$.

While $\mu'_\alpha(\boldsymbol{r})$ and $a'_{\alpha\beta}(\boldsymbol{r})$ can change as environmental conditions fluctuate [37] (Fig. S3), we will generally focus on their values in an equilibrium environment $\boldsymbol{r}^*$, *i.e.* $a'_{\alpha\beta}(\boldsymbol{r}^*)$ and $\mu'_\alpha(\boldsymbol{r}^*)$ (Fig. 2c,d). Under these conditions, they can be treated as effective gLV parameters through the algebraic correspondence between Eqs. 6 and 1. Beyond this point, we will suppress the explicit dependency on $\boldsymbol{r}^*$ for notational compactness.

In previous studies, the stability of such two-population mutualisms has been investigated through modified gLV equations that introduce new quantities – for example, terms that cause facilitation to saturate or become competitive as the donor's density increases [22, 50]. These modifying terms are, in effect, intended to impose non-linear density-dependencies on top of the linear density-dependencies of the Lotka-Volterra model that more realistically represent

the mechanisms underpinning the mutualism. However, as interaction mechanisms are not explicitly represented in such models, the proposed relationship between mechanisms and effective gLV parameters remains a choice that must be intuited by the modeller. By contrast, the mechanistically explicit mapping between Eqs. 1 and 6 allows us to avoid this intuitive leap. How does this affect our understanding of the stability of mutualisms?

To investigate this question, we asked how the biotic accelerations $a'_{\alpha\beta}$ and abiotic accelerations μ'_α (which are algebraically homologous to interaction strengths $a_{\alpha\beta}$ and intrinsic growth rates μ_α respectively) vary as the amino acid production rate ℓ_w is increased, representing an evolutionary scenario in which one population unilaterally modifies its cross-feeding strategy [51]. From a naïve interpretation of the gLV model, we would expect this to result in stronger positive interactions from the producer to the consumer, while the costs associated with amino acid production would drive increasingly negative intrinsic growth rates for the producer [10, 21].

To test whether this prediction held in our mechanistic model, we allowed the simulated chemostat to reach an equilibrium for each value of ℓ_w and recorded the equilibrium densities of $\mathring{v}$ and $\mathring{w}$ (Fig. S4a, lines), biotic accelerations $a'_{\mathring{v}\mathring{v}}$, $a'_{\mathring{v}\mathring{w}}$, $a'_{\mathring{w}\mathring{w}}$ and $a'_{\mathring{w}\mathring{v}}$ (Fig. 3a) and abiotic accelerations $\mu'_{\mathring{v}}$ and $\mu'_{\mathring{w}}$ (Fig. 3b). Surprisingly, while the biotic accelerations were initially positive, they switched signs to negative as the strength of the cooperative mechanism was increased. By contrast, the abiotic accelerations grew in value, becoming increasingly positive after being negative at low production rates. While these relationships were unexpected, the accelerational analogue of the expression relating equilibrium densities to gLV parameters ($\boldsymbol{x}^* = -\boldsymbol{\mu}' A'^{-1}$) accurately yielded the equilibrium densities $\boldsymbol{x}^*$ (Fig. S4a, circles), confirming the algebraic correspondence between Eqs. 1 and 6. We also found that the real part of the system's eigenvalue spectrum was negative for all production values (Supplementary Note 1.3.2, Fig. S5), indicating linear stability of coexistence (Fig. S4b). These results are not an artefact of the small size of the community or the choice of mechanistic parameters, as they generalise to larger communities with random parameters [52] (Fig. S6). This suggests that our intuitive understanding of the relationship between interaction mechanisms and effective gLV parameters is flawed: increased cross-feeding leads to stronger mutual growth but also stronger competition.

To gain a deeper understanding of the processes driving this paradoxical relationship, we turned to the scalar fields representing the inter-specific biotic acceleration $a'_{\mathring{v}\mathring{w}}$ (Fig. 3b) and the

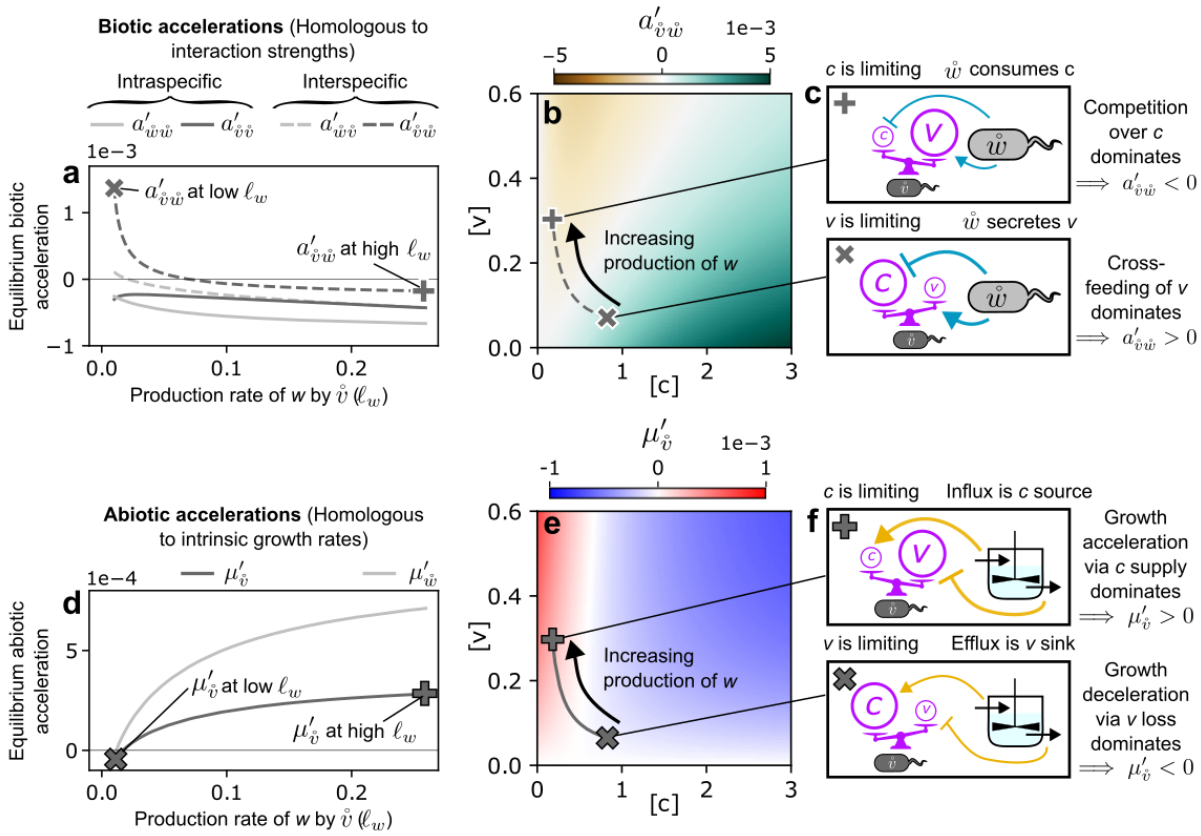

Figure 3: **Modulation of auxotroph amino acid production rates causes counter-intuitive changes to effective gLV parameters.** a,d) Keeping all other parameters fixed, we varied the rate at which $\mathring{v}$ converts the carbon source to secreted w, ℓ_w, and numerically simulated each chemostat's dynamics until it reached an equilibrium. We then evaluated the equilibrium biotic accelerations for each pair of populations (a) and abiotic accelerations for each population (d). b,e) Counter-intuitive relationships between the varying strength of the cooperative cross-feeding mechanism and the effective gLV parameters can be understood by plotting the changing position of $\boldsymbol{r}^*$ on the scalar fields representing one of the biotic (b) and abiotic (e) accelerations (replotted from Fig. 2 e and f). c,f) Schematics representing the mechanisms driving changes in effective gLV parameters under different production rates of w. $\times$ and $+$ symbols represent simulations with the lowest and highest production rates of w, respectively. Dilution rate $D = 0.01$.

abiotic acceleration $\mu'_{\mathring{v}}$ (Fig. 3e). We selected these over $a'_{\mathring{w}\mathring{v}}$ and $\mu'_{\mathring{w}}$ as they are independent of ℓ_w and thus remain fixed over the parameter sweep. As the production of w increases, the equilibrium concentration of c decreases while the concentration of v increases, driven by the increased density of the w auxotroph. In the low production scenario, the concentration of the amino acid is growth limiting and cross-feeding of v from $\mathring{w}$ dominates over competition for carbon, leading to a positive net value of $a'_{\mathring{v}\mathring{w}}$. By contrast, carbon limitation in the high production scenario leads to dominance of carbon-based competition between the two strains, creating a negative net value (Fig. 3c). A similar argument applies to the abiotic accelerations, but with the effect of the external processes (*i.e.* the fluxes of chemicals into and out of the chemostat) substituted in place of the mutualistic partner; domination of loss of amino acids through the system's efflux drives a negative net value of $\mu'_{\mathring{v}}$ in the amino-acid limited low production scenario, while the positive growth rate impact of the carbon supply dominates in the carbon-limited high production scenario (Fig. 3f).

2.3 How nutrient exchanges shape coexistence: mapping mechanisms to MCT

With a clearer understanding of the relationship between mutualistic mechanisms and effective gLV parameters, we are now equipped to move one level higher and understand how mechanisms shape coexistence. Two-population ecosystems have been extensively studied through the lens of Modern Coexistence Theory (MCT), which seeks to partition processes that impact coexistence outcomes into stabilising components that reduce the niche overlap between populations and equalising components that balance the fitness ratio between populations [29]. A classic result arising from two-population Lotka-Volterra models is that explicit expressions for the niche overlap ρ and fitness ratio $\frac{k_1}{k_2}$ can be obtained from the gLV parameters (Supplementary Note 1.3.3) [53, 54]:

$$\rho = \sqrt{\frac{a_{12}a_{21}}{a_{11}a_{22}}} \tag{7a}$$

$$\frac{k_1}{k_2} = \frac{\mu_1}{\mu_2}\sqrt{\frac{a_{22}a_{21}}{a_{11}a_{12}}}. \tag{7b}$$

where 1 and 2 are labels for the two populations. Coexistence is feasible only if

$$\rho < \frac{k_1}{k_2} < \frac{1}{\rho}. \tag{8}$$

We can define an accelerational analogue of this expression. Using the labels of the auxotrophs, we obtain:

$$\rho' = \sqrt{\frac{a'_{\mathring{v}\mathring{w}} a'_{\mathring{w}\mathring{v}}}{a'_{\mathring{w}\mathring{w}} a'_{\mathring{v}\mathring{v}}}} \tag{9a}$$

$$\frac{k'_{\mathring{w}}}{k'_{\mathring{v}}} = \frac{\mu'_{\mathring{w}}}{\mu'_{\mathring{v}}} \sqrt{\frac{a'_{\mathring{v}\mathring{v}} a'_{\mathring{v}\mathring{w}}}{a'_{\mathring{w}\mathring{w}} a'_{\mathring{w}\mathring{v}}}}. \tag{9b}$$

Mutualisms have previously been thought to be incompatible with this form of MCT, as positive intraspecific interaction strengths lead to imaginary niche overlaps [55]. However, we have already shown that values of $a'_{\alpha\beta}$ are negative for most amino acid production rates, suggesting that we may be able to use this framework to analyse many instances of the cross-feeding system.

To test whether we could use this approach to shed light on the mechanistic basis of coexistence in this system, we manipulated the amino acids through two mechanisms: varying their concentrations in the input media r_{IN} (Fig. 4a-c) and varying their production rates by the two populations (Fig. 4d-f). We then scored communities based on whether one, both or neither population was able to persist at equilibrium (Fig. 4b,e). Finally, we mapped these scenarios onto niche overlap and fitness ratio axes using Eq. 9b to verify the accuracy of the coexistence predictions by MCT (Fig. 4c,f). Some communities displayed positive biotic accelerations, which were excluded from the niche overlap and fitness ratio calculations to avoid imaginary values. These tended to be located at the edges of the coexistence regions where amino acid concentrations were particularly limiting. For the remaining communities, we found that Eq. 9b precisely predicts the coexistence properties of this system, with combinations of mechanistic parameters that result in competitive exclusion mapped to the boundaries of the coexistence region. This boundary-mapping effect is a generic feature of MCT when applied to two-species EO models through Eq. 9b (Supplementary Note 1.4).

How do coexistence outcomes change as underlying mechanisms are varied? Changes in the

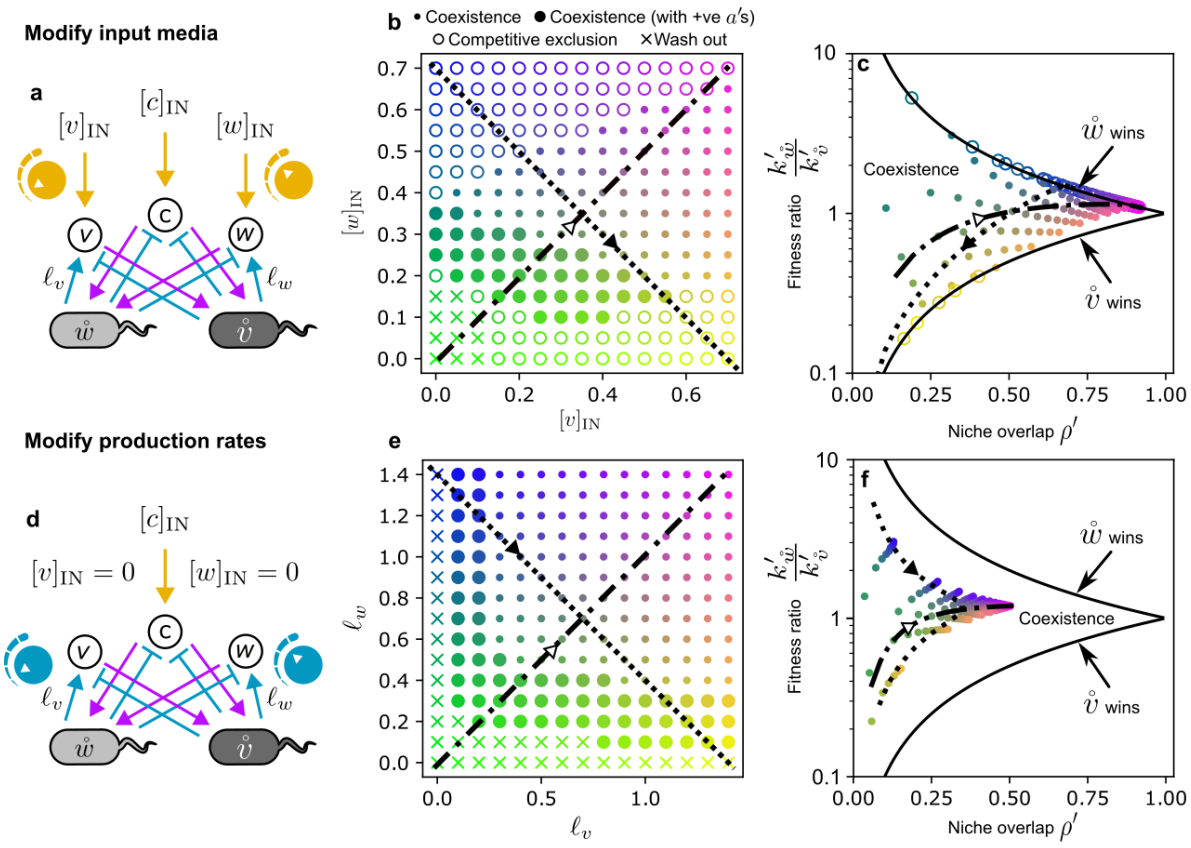

Figure 4: **Mapping interaction mechanisms onto modern coexistence theory** a) To test the validity of our accelerational definition of the niche overlap and fitness ratio, we first varied the input concentrations of the two amino acids in the two population auxotrophy model. b) We then performed numerical simulations of the population dynamics in the chemostat for each combination of input concentrations, scoring coexistence outcomes based on whether both populations were washed out (crosses), one population competitively excluded the other (open circles) or both populations stably coexisted (filled circles). c) The abiotic and biotic accelerations for both strains in the equilibrium environment $\boldsymbol{r}^*$ were then converted to niche overlaps ρ' and fitness ratios $\frac{k'_{\mathring{w}}}{k'_{\mathring{v}}}$ (main text). Solid lines indicate predicted coexistence boundaries (Eq. 8). Note that the contours of constant input amino acid ratio (dot-dash line) and total input amino acid concentration (dotted line) are mapped onto the niche overlap and fitness ratio axes. d-f) Equivalent analysis conducted by varying amino acid production rates from the two auxotrophs. Large filled circles in b and e denote stably coexisting communities with at least one positive biotic acceleration a', which are excluded from the niche overlap and fitness ratio axes in c and f. Simulations resulting in mutual wash out are also excluded from these axes. Points with matching colours in b, c and e, f correspond to the same simulation in the two panels. Dilution rate $D = 0.03$, input media contains no amino acids in d-f.

ratio of the input amino acid concentrations $[v]_{\mathrm{IN}}$:$[w]_{\mathrm{IN}}$ (Fig. 4b,c, dashed line with black arrowhead) predominantly drove changes in fitness ratios, with the less supported population being outcompeted as soon as the system hit a coexistence boundary. On the other hand, increasing the total amino acid concentration while keeping their ratio fixed (Fig. 4b,c, dot-dashed line with white arrowhead) mainly changed the niche overlap, leading to a progression from mutual wash-out to coexistence and finally competitive exclusion as observed in experiments [24].

A similar analysis on amino acid production rates (Fig. 4e,f) yielded closely related patterns. However, we found that no combination of production rates resulted in competitive exclusion, reflecting the mutual dependence of the populations in media lacking amino acids. Instead, correlated changes in the niche overlap and fitness ratio prevented the system from hitting the coexistence boundary (Fig. 4f). An EO model representing facultative cross-feeding [9] displayed an inverted relationship between nutrient production and niche overlap, while also allowing competitive exclusion to arise at high nutrient production rates (Fig. S7, Table S3). This suggests that it is the structure of the auxotrophy system (cooperation through exchange of essential resources and competition over a shared resource) rather than cross-feeding *per se* that drives the observed trends.

We now investigated the mechanistic basis for these patterns. Adopting a sampling-based approach, we generated communities with randomised amino acid production rates and input concentrations and scored the fitness ratio and niche overlap of each pair of strains at equilibrium. We then binned auxotrophic communities according to their values of these two quantities and calculated the average nutrient concentrations, mechanistic parameters (Fig. 5a-g) and effective gLV parameters (Fig. S8) for all systems falling within these bins. This allowed us to relate variations in the MCT metrics to underlying mechanistic processes (Fig. 5f): at low amino acid concentrations, the two populations are not competing for the carbon source as their growth is limited by different amino acids. Processes that increase amino acid concentrations relieve this non-competitive growth constraint and instead shift the populations towards competition for the carbon source on which they are mutually dependent, driving an increase in niche overlap (Fig. 5a-c). Fitness ratios on the other hand are determined by the relative fluxes of the two amino acids, with imbalanced fluxes favouring the auxotroph receiving the stronger supply of their limiting nutrient (Fig. 5d-g).

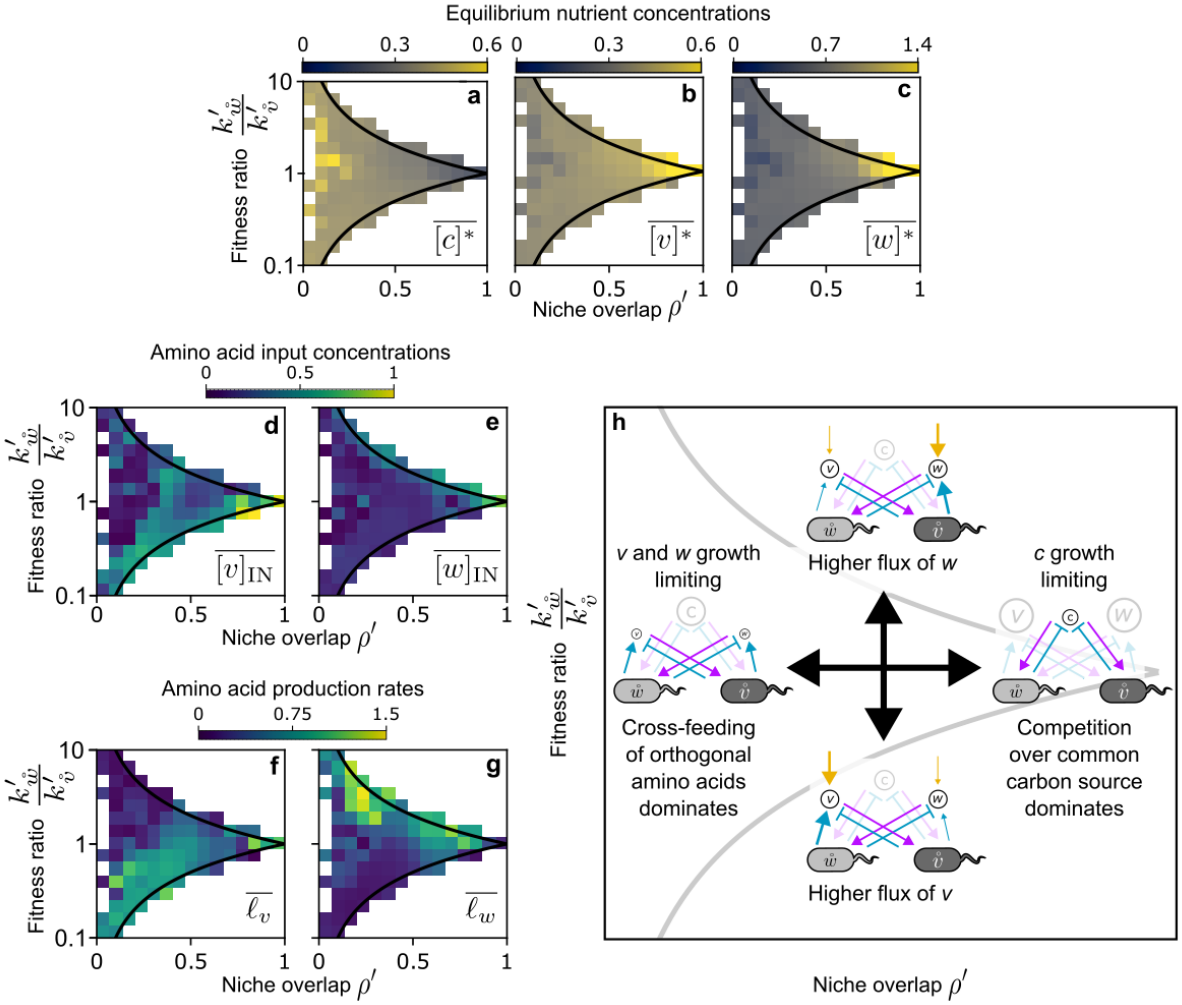

Figure 5: **The mechanistic basis of fitness ratios and niche overlaps of auxotrophic bacteria.** a-g) We generated communities with randomised combinations of amino acid production rates and amino acid input concentrations and evaluated the niche overlap ρ' and fitness ratio $\frac{k'_{\mathring{v}}}{k'_{\mathring{w}}}$ for each community at equilibrium. We then binned communities along these axes and calculated the average equilibrium carbon source concentration $\overline{[c]^*}$ (a) and amino acid concentrations $\overline{[v]^*}$, $\overline{[w]^*}$ (b,c), as well as the amino acid input concentrations $[w]_{\mathrm{IN}}$, $[w]_{\mathrm{IN}}$ (d,e) and production rates $\overline{\ell_v}$, $\overline{\ell_w}$ (f,g) for all communities falling within each bin. h) Summary of mechanisms driving changes in niche overlap and fitness ratios in the auxotrophy model. As in Fig. 4, communities with positive biotic accelerations were excluded from the analysis. Dilution rate $D = 0.03$.

This perspective also allows us to explain why the system responds differently when the imbalance in fluxes arises due to internal (production rates) versus external (input concentrations) changes in mechanisms. Similar to Song *et al.* [56], we find that mechanistic changes are not purely stabilising nor equalising. Introducing an imbalance in production rates leads to an imbalance in the fitness ratio. However, it also leads to weaker overall growth due to the mutual dependence of the populations. This in turn leads to lower niche overlap due to less competition for carbon, allowing coexistence to be maintained (dotted line in Fig. 4f). Similar patterns have been observed experimentally, with increased production of an amino acid by one member of a cross-feeding mutualism favouring the recipient but never leading to competitive exclusion [47]. On the other hand, imbalances in externally supplied amino acid concentrations are not subject to this internal regulation through changes in niche overlap. This allows imbalances in the fitness ratio to drive the system into the coexistence boundary, enabling competitive exclusion (dotted line in Fig. 4c).

2.4 Application of MCT through our framework allows prediction of coexistence outcomes based on known interaction mechanisms

As a final test of our framework, we decided to investigate whether it captured coexistence outcomes in experimental communities. In Ho *et al.* [57], the physiology of each member of a 15-member gut community was characterised individually by quantifying their impact on $\approx 16,000$ metabolomic markers in rich media. These monoculture measurements were then used to construct a coarse-grained EO model which accurately predicted the outcome of multi-species competition experiments (Fig. S9). The resulting model is built from impact and sensitivity functions for each species that fully characterise the mechanisms through which they interact (Methods), providing the raw ingredients for application of our framework.

We implemented this model and cross-validated the analytical framework by applying it to an independent dataset quantifying interactions between all 12 members of the OMM 12 gut community [58], resulting in a second coarse-grained EO model (Methods, Fig. S10). These monoculture-derived models were used to map each pair of species to the MCT axes. On the same axes, we also scored each point based on the outcome of independent competition experiments between the corresponding species pair (Fig. 6a). Across both model systems, we found that the median species pairs exhibiting competitive exclusion was mapped to a location

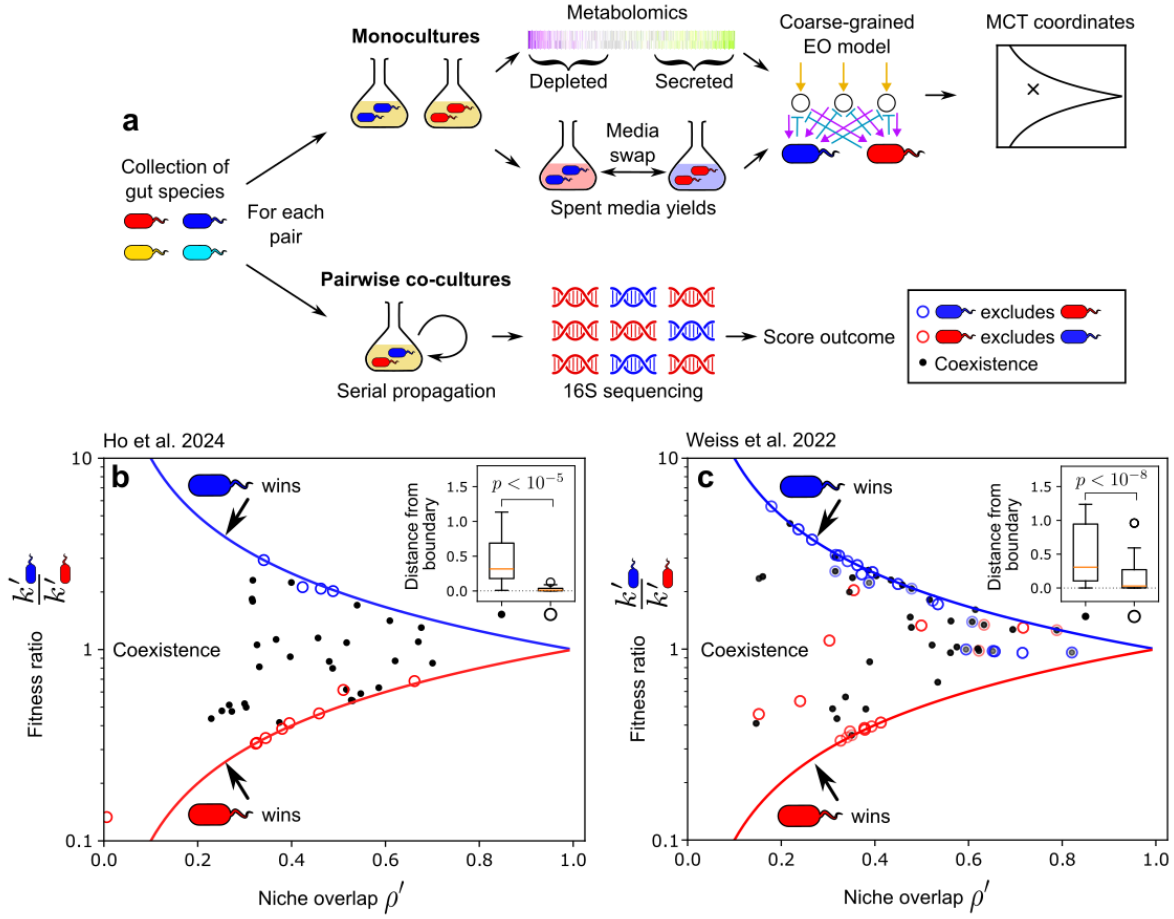

Figure 6: **MCT allows prediction of coexistence outcomes in experimental gut communities.** To evaluate the utility of our framework for understanding coexistence in experiments, we applied it to *in vitro* data from two simplified gut communities [57, 58]. a) Monoculture metabolomic and spent-media experiments permitted construction of coarse-grained EO models representing competition between pairs of species. We used our framework to map the output of these models onto the niche overlap/fitness ratio axes for each simulated species pair (upper). This was compared to the outcome of serial transfer experiments conducted on the pair (lower). b,c) Outcome of MCT analysis. Points corresponding to competitive exclusion (open circles) were significantly closer to the coexistence boundaries (solid lines) than points corresponding to coexistence (solid circles) (insets). Distances are measured to corresponding coexistence boundary for pairs exhibiting competitive exclusion or a randomly selected coexistence boundary for coexisting pairs. Assignment of strains in each pair as blue or red was random. Fitness ratios were log-transformed during calculation of distances.

$13.5\times$ closer to the coexistence boundary than the median coexisting pair (Fig. 6b,c), a highly significant result ($p < 10^{-5}$ and $p < 10^{-8}$ for Ho *et al.* [57] and Weiss *et al.* [58] respectively, Mann-Whitney U test). We also found that the derived statistics were biologically meaningful, with a weak but significant negative correlation between genomic distance and niche overlap as observed in previous studies (Fig. S11) [59]. These results show that application of MCT through our framework is a powerful tool for simplifying our understanding of ecosystem composition, compressing interaction mechanisms involving tens of thousands of different chemical mediators into two numbers that almost completely capture coexistence outcomes [60].

3 Discussion

The relative roles of cooperation versus competition in ecosystems is a long-debated topic in ecology [14–16, 61–63]. Within microbiology, this controversy is perhaps best reflected in the apparently contradictory results of studies that measure interaction strengths, which are predominantly competitive [64], versus those that study interaction mechanisms, which find widespread mutualistic exchanges [2]. Our results reconcile these two camps by emphasising that cooperative and competitive processes often occur simultaneously, with the net outcome depending on the environmental and community context [37]. The auxotrophy system that we model here is a paradigmatic obligate mutualism in terms of the ability of the two strains to persist (Fig. S1). Yet when we look at the quantities algebraically equivalent to the interaction strengths of the gLV model $a_{\alpha\beta}$, the biotic accelerations $a'_{\alpha\beta}$, we observe that competition dominates and becomes stronger as cross-feeding is strengthened (Fig. 3). This is generally expected to stabilise communities [11, 12]. Cross-feeding communities can thus be mutualistic in their persistence properties, but competitive when responding to small perturbations.

In line with these results, previous studies have shown that the restraining effect of competition over shared resources can prevent mutualisms from destabilising ecosystems. Aside from carbon availability, these limiting factors can include nitrogen, space and the density of shared partners [11, 34, 46, 65]. Similar arguments have also been made for groups of macroscopic organisms, such as complexes of Müllerian mimics that compete for nectar [66]. However, an important outstanding question in the context of gLV-type models is why this enhanced competition does not also suppress population sizes. Our results show that increased competition is compensated for by a paradoxical increase in the term that plays the role of the intrinsic growth

rates μ_α, the abiotic accelerations μ'_α (Fig. 3). This finding contrasts with the typical assumption that μ_α is either fixed or declines with increasing costs of cooperation, demonstrating that though algebraically equivalent at equilibrium, the gLV and aEO equations have fundamentally different interpretations. Indeed, there is nothing 'intrinsic' about μ'_α, which is largely determined by the extrinsic environmental inputs. Studies which assume that intuitive relationships hold between interaction mechanisms and effective gLV parameters should be revisited in light of this alternative interpretation.

These findings also impact our understanding of the niche overlap and fitness ratio metrics of MCT. While our results are consistent with previous geometric interpretations of niche overlap as the degree of alignment between requirements or impacts of populations [28, 30, 53], our interpretation of the fitness ratio is more difficult to reconcile with existing work; certainly it is not obvious how to interpret the observed relationships as variations in fitnesses. While our findings suggest that it represents the extent to which fluxes of environmental quantities favour a particular population (Fig. 5h), additional EO models should be interrogated to assess the universality of this interpretation.

The main technical advance of our work is the derivation of a general and exact method for transforming mechanistic ecosystem models into a gLV-like parametrisation, allowing tools used to analyse gLV systems to be applied to mechanistic models. For example, we have shown that this insight can be used to apply MCT to multiple different EO models (Figs. 4-6), generalising previous findings [28]. MacArthur's solution to this problem, based on the assumption that resources equilibrate much more rapidly than populations [26], has dominated the literature since its discovery [53, 56, 67–69]. However, this technique is approximate and can only be applied in cases where the dynamics of resources are logistic [27], a serious limitation when modelling the dynamics of ecosystems based on abiotic nutrients such as microbiota. Our approach avoids eliminating this timescale of the environmental dynamics, consequently resulting in a second-order description of the population dynamics. It remains to be seen whether this accelerational picture proves a more accurate description of real ecosystems than existing rate-based representations, although we note that changes in population growth rates (*i.e.* growth accelerations) in closed microcosms are accurately described by a limiting case of the aEO equation [37]. Second-order descriptions also enable replication of phenomena not observed in standard first-order systems, such as density oscillations of single populations and time lags

in population responses [70–72].

Our results also suggest new methods for analysing experimental communities with mechanistic frameworks. In this and previous work [37], we have made predictions of microbial community dynamics under the assumption that we have extensive knowledge of underlying interaction mechanisms. This knowledge is encoded through explicit representations of the impact, sensitivity and allogenic functions. Unfortunately, characterising these functions is typically not straightforward, as it requires extensive measurements of the relationship between microbes and their chemical environment [57, 73]. However, Eq. 6 suggests a solution to this problem: while it takes the environmentally-mediated interaction structure of microbial communities into account, the interaction mechanisms are contained within the effective gLV parameters $a'_{\alpha\beta}(\boldsymbol{r}^*)$ and $\mu_\alpha(\boldsymbol{r}^*)$. Appropriate modifications of techniques for measuring gLV parameters – such as characterisation of the density-dependence of growth rates [74] – may permit quantification of these effective parameters without requiring measurements of environmental factors. This would allow us to characterise the properties of equilibrium communities with comparatively simple population growth measurements.

While our approach opens many new avenues of investigation, it also has its drawbacks. One of the main attractions of the gLV model and related frameworks are their analytical tractability, forming the basis of a large body of results based on random matrix theory [11, 12, 75]. These results describe the properties of very large communities provided that the associated parameters follow prescribed statistical patterns. By contrast, our approach relies heavily on numerical integration schemes to solve system dynamics and obtain equilibrial environments $\boldsymbol{r}^*$ for which Eq. 6 holds. Although techniques exist for calculating $\boldsymbol{r}^*$ analytically for specific models (Supplementary Note 1.2), these generalise poorly and typically require explicit evaluation of matrix inverses. They also assume *a priori* that such a point exists and is an attractor, rather than the system dynamics converging on indefinite oscillations or chaos. Application of random matrix theory through this framework is therefore likely to be challenging.

In summary, our results provide a highly flexible link between the molecular mechanisms underpinning interactions and emergent coexistence outcomes. Application of this framework to the question of how interaction mechanisms constrain ecosystems promises to resolve a number of outstanding problems in ecology beyond the paradox that we address here. Successfully addressing these problems will provide new tools for understanding and manipulating ecosystems

across scales, including microbiomes.

4 Methods

4.1 Model definitions

4.1.1 Auxotrophy model

Species in the auxotrophy model depend on both an in-common carbon source that all members of the community rely on (*e.g.* glucose) and a species-specific amino acid that they alone rely on [52]. The co-essentiality of these two resources is represented by using the product of separate Monod functions for the two resources when determining growth rates and resource utilisation rates. We additionally include a metabolic shunt that enables production of cross-fed amino acids even when the essential amino acid for a given species is not available [48]. This ensures that amino acid secretion is not directly coupled to growth, allowing the community to begin secreting amino acids into the input media even when it contains only the raw carbon source. The community can thus establish in amino-acid free media (Fig. S1). The rate of amino acid secretion is determined purely by the carbon source availability, again transformed via a Monod function.

We arrange the environment vector $\boldsymbol{r}$ so that amino acid in position ρ corresponds to the amino acid required by the species with the same index (*i.e.* so that $\rho = \alpha$ for auxotroph α and required amino acid ρ). The in-common carbon source is placed in the final position of the vector with index $N+1$ (where N is the number of auxotrophic populations). The sensitivity function is then defined as:

$$g_\alpha = \nu_\alpha \frac{r_\alpha}{r_\alpha + K_{\alpha\alpha}} \frac{r_{N+1}}{r_{N+1} + K_{\alpha(N+1)}} - D, \tag{10}$$

where D is the dilution rate of the chemostat, $K_{\alpha(N+1)}$ and $K_{\alpha\alpha}$ are the half-velocity constants for the carbon source and consumed amino acid respectively and ν_α is the maximal growth rate.

The impact function is additionally defined as:

$$f_{\alpha\rho} = \begin{cases} -\frac{1}{Y_{\alpha\rho}}\nu_\alpha \frac{r_\rho}{r_\rho + K_{\alpha\rho}} \frac{r_{(N+1)}}{r_{(N+1)} + K_{\alpha(N+1)}} & \text{if } \rho = \alpha \text{ } (\rho \text{ is missing amino acid}) \\ -\frac{1}{Y_{\alpha\rho}}\nu_\alpha \frac{r_\alpha}{r_\alpha + K_{\alpha\alpha}} \frac{r_\rho}{r_\rho + K_{\alpha\rho}} - \nu_\alpha \frac{r_\rho}{r_\rho + K_{\alpha\rho}} \sum_{\gamma \neq \{\alpha, N+1\}} \ell_{\alpha\gamma} & \text{if } \rho = N+1 \text{ } (\rho \text{ is carbon source}) \\ \nu_\alpha \ell_{\alpha\rho} \frac{r_{(N+1)}}{r_{(N+1)} + K_{\alpha(N+1)}} & \text{otherwise } (\rho \text{ is secreted amino acid}) \end{cases} \tag{11}$$

where we have introduced the scaled production rate of amnio acid ρ by species α as $\ell_{\alpha\rho}$ and the yield of species α on amino acid/carbon source ρ as $Y_{\alpha\rho}$.

Finally, we define the allogenic function using the standard form for chemostat-type systems, $\boldsymbol{\sigma} = D(\boldsymbol{r}_{\text{IN}} - \boldsymbol{r})$, where $\boldsymbol{r}_{\text{IN}}$ is the composition of the input media.

We provide parameter values for the two-species auxotrophy model in table S2. In some cases, we suppress the species label where this is clear from context to simplify notation (for example, $\mathring{v}$ is the only species that secretes w, so we write ℓ_w rather than $\ell_{\mathring{v}w}$). Note that some parameters (ℓ_v, ℓ_w, D, $[v]_{\text{IN}}$ and $[w]_{\text{IN}}$) are modified during some analyses, in which case they are specified on plot axes, in the relevant figure's caption, or were drawn randomly (see next section).

4.1.2 Facultative cross-feeding model

We modified an existing model of cross-feeding of substitutable resources [9]. Species consume all available resources at a rate that is linearly proportional to their concentration and a resource preference parameter $q_{\alpha\rho}$. Each consumed resource is converted into the other resources at a conversion rate $\phi_{\alpha\rho\gamma}$, where ρ is the consumed resource and γ is the target resource.

The sensitivity function for this model is

$$g_\alpha = \sum_\rho r_\rho q_{\alpha\rho}(1 - \sum_\gamma \phi_{\alpha\rho\gamma}) - D, \tag{12}$$

while the impact function is

$$f_{\alpha\rho} = -q_{\alpha\rho} r_\rho + \sum_\gamma \phi_{\alpha\rho\gamma} q_{\alpha\gamma} r_\gamma. \tag{13}$$

Note that the term $(1 - \sum_\gamma \phi_{\alpha\rho\gamma})$ in the sensitivity function enforces conservation of mass by ensuring that total resource exchange by α plus total growth of α is equal to one. As for the auxotrophy model, we defined the allogenic function using the standard chemostat definition $\boldsymbol{\sigma} = D(\boldsymbol{r}_{\text{IN}} - \boldsymbol{r})$.

Parameters for the two-species model shown in Fig. S7 are specified in S3 or are specified on the figure's axes. Axes in Fig. S7b ('$\mathcal{A}$ conversion fraction' and '$\mathcal{B}$ conversion fraction') denote the fraction of the absorbed resources converted into the other type and re-secreted ($\phi_{\alpha\rho\gamma}$) for the indicated species.

4.1.3 Gut community consumer-resource model

Ho *et al.* [57] constructed a coarse-grained consumer resource model based on explicit measurement of metabolomic impacts of species on their media and their growth in the spent media of other species. We directly implemented this model, modifying it so that simulated communities were grown in a chemostat rather than a serial-transfer system as in the original publication. This model was also used to simulate species characterised in Weiss *et al.* [58].

The model can be written in EO form as follows:

$$g_\alpha = \sum_\rho q_{\alpha\rho} r_\rho - D, \tag{14}$$

$$f_{\alpha\rho} = -q_{\alpha\rho} r_\rho, \tag{15}$$

where $q_{\alpha\rho}$ represents an empirically-derived resource preference. We also defined the allogenic function using the standard chemostat definition $\boldsymbol{\sigma} = D(\boldsymbol{r}_{\text{IN}} - \boldsymbol{r})$.

4.2 Simulations

SciPy's `solve_ivp` function was used to numerically integrate the resulting systems of coupled ODEs using the Runge-Kutta method of order 5(4). We built a Python module (EOsimSuite) to facilitate rapid and flexible implementation of EO simulations based on defined impact, sensitivity and allogenic functions. Jupyter notebooks containing all code necessary to reproduce the models presented in this manuscript are available here.

4.2.1 Auxotrophy model: parameter sampling and setup

Parameters for the randomly sampled mechanistic sweep (Figs. 5, S8) were selected from uniform distributions. The amino acid production rates ℓ_v and ℓ_w were drawn from the range $[0, 1.5]$, while the input concentrations v_{IN} and w_{IN} were drawn from the range $[0, 1]$. The dynamics of the resulting model was numerically integrated until reaching an equilibrium state. The resulting system was then mapped onto niche overlap and fitness difference axes (Supplementary Note 1.3.3) and placed into a 15×15 grid covering the niche overlaps between 0 and 1 and the fitness differences between 0.1 and 10. Mechanistic parameters (Fig. 5 and effective gLV parameters (Fig. S8) were binned according to the position of the final system in this grid. Systems that fell outside this region (including systems with positive values of $a'_{\alpha\beta}$, see main text) were excluded from further analysis. This procedure was repeated 100,000 times, building up a collection of underlying parameters for each bin. The collection in each bin was then averaged to give the final heatmaps.

For the randomly parameterised 5-species model presented in Fig. S6, we drew the values of $K_{\alpha\rho}$, $Y_{\alpha\rho}$, ν_α and $\ell_{\alpha\rho}$ from random distributions. $K_{\alpha\rho}$s were drawn uniformly from the range $[0.75, 1.25]$. $Y_{\alpha\alpha}$s (the yield of the amino acids) were drawn uniformly from the range $[15, 25]$, while $Y_{\alpha,(N+1)}$ (the yield of the carbon source) was set at 1. ν_αs were drawn from $[9, 11]$. $\phi_{\alpha\rho}$s was constructed by drawing values uniformly from the range $[-0.1, 0.4]$ and clipping the negative part of the resulting distribution to zero, simulating amino acids that are not produced by α. We additionally set $\phi_{\alpha\alpha} = 0$ to prevent secretion of the amino acid α was auxotrophic for and $\phi_{\alpha(N+1)} = 0$ to prevent secretion of the carbon source. The resulting set of random values was scaled by a constant that allowed us to vary the average production rate, which was swept systematically from 0.001 to 0.3. The 'average production rate' is the average of all production rates following this scaling. We fed the simulated community in the chemostat on media containing the carbon source at concentration $r_{(N+1)} = 1$ and no amino acids. All populations were inoculated at density 0.05. The dilution rate D was 0.05.

4.2.2 Cross-feeding model with substitutable resources: setup

For the parameter sweeps shown in Fig. S7, we grew each simulated community in a chemostat fed with media containing both substitutable resources at concentration 0.3. Both populations were inoculated at density 1. The dilution rate D was 0.05.

4.2.3 Gut consumer-resource models

Coarse-grained resource preferences $q_{\alpha\rho}$ and input media compositions $\boldsymbol{r}_{\text{IN}}$ were set using fitted values provided in [57] or as indicated in section 4.3.1. The dilution rate D was set at $0.11\ h^{-1}$ (for Ho *et al.* [57]) or $0.192\ h^{-1}$ (for Weiss *et al.* [58]), calculated as the equivalent long-term exponential dilution rates to the original serial propagation assays. We simulated each community for which there was a corresponding serial propagation experiment, setting the stating population size for each species present in the inoculum as 1 and all other species as 0. Each system was simulated for $240\ h$ or $72\ h$ – corresponding to the duration of the original serial propagation experiments – and final abundances and effective gLV parameters extracted.

For Fig. S9, final simulated abundances were normalised to generate relative abundances and compared to the final relative abundances in corresponding serial propagation experiments. In Fig. 6, we scored the coexistence outcome for a given species pair as competitive exclusion if one of the two populations had a relative abundance of less than 5% after the final transfer.

Some pairs of species in Ho *et al.* [57] (58 out of 105) had no overlap in their coarse-grained resource preferences due to application of a stringent model complexity cutoff during parameter fitting in the original publication. Such cases generally involved low-growth species, which had small impacts on their media and were consequently weighted weakly during model fitting. These combinations were excluded from Figs. 6 and S11. In addition, final abundances in the serial propagation experiment were not reported for three of the pairs in this study. These were excluded from Fig. 6 but were included in Fig. S11.

4.3 Data analysis

4.3.1 Generation of coarse-grained consumer resource model

We modified the approach developed in Ho *et al.* [57] to parametrise a coarse-grained consumer-resource model describing the 12-member OMM 12 community. All datasets used during this procedure are presented in the original publication [58]. The inputs to the pipeline consisted of two datasets. Firstly, OD600-based growth curves were obtained and used to evaluate the maximal density of all pairwise co-cultures ($x_{\alpha\beta},\ n = 132$), monocultures in fresh media ($x_{\alpha},\ n = 12$),

and monocultures of all strains (β) grown in the spent media of every other strain α ($x_\beta^\alpha, n = 144$). Secondly, we compiled a list of metabolic features that were significantly depleted or enriched by the activity of each strain, as assessed via comparison of untargeted mass spectrometry of fresh and spent media (Fig. S10a). Crucially, direct co-cultures did not feature in the input data; any growth impacts of strains on one another were mediated indirectly through spent media exchanges.

The model contains 3 sets of parameters which were fitted to these monoculture datasets: the number of coarse-grained resource pools (P), their concentrations in the environmental input ($\boldsymbol{r}_{\text{IN}}$) and the species-specific consumption rates of each coarse-grained resource pool ($q_{\alpha\rho}, \alpha = 1, \ldots, 12,\ \rho = 1, ..., P$). We simplified this final group of parameters by assuming that each species consumed resources from all the coarse-grained pools it could utilise at a uniform species-specific rate q_α^*. To infer these parameters, we first excluded metabolites that were enriched, considering only those that were depleted. All metabolic features that were depleted by the same set of strains were then clustered into coarse-grained resource groups. The 12 resource groups that were depleted by just one of each of the 12 strains were retained, and the remaining groups sorted by the number of metabolic features assigned to each (Fig. S10b). We now iterated a least-square fitting procedure over these ordered groups, retaining increasingly low-scoring groups at each step. The 156 monoculture yields (12 in fresh + 144 in spent media) were the dependent variables in these regressions, while $\boldsymbol{r}_{\text{IN}}$ were the fitted parameters.

Our approach to these regressions differed from that of Ho *et al.* [57] in one key regard. The competition residues (defined as $\Delta_{\alpha\beta} = x_\alpha + x_\beta^\alpha - x_{\alpha\beta}$) were not zero-centred for our data, but shifted with an approximate mean of 0.3 (Fig. S10c). This suggests that either metabolite-mediated interactions cannot fully explain the data or that the OD signal saturates at high population densities. To improve fitting, we applied a correction based on the competition residues. Rather than performing the fitting of the input resource concentrations directly on the population densities in spent media x_β^α, we applied a correction based on the residual $x_\beta^\alpha - W\Delta_{\alpha\beta}$ and iterated the least-square fitting procedure through both the number of coarse-grained resource pools ($P = 12, \ldots, 80$) and the size of the correction weight ($W = 0, 0.2, \ldots, 1$, Fig. S10d). This resulted in (6x69) 414 models from which we selected the one with lowest AIC ($P = 25$ and $W = 0.6$) and extracted the inferred values of $\boldsymbol{r}_{\text{IN}}$ (Fig. S10e). Finally, we fitted the monocul-

ture growth curves to a sigmoid function and extracted the strain-specific maximum growth rate (λ_α). The resource utilisation rates q_α^* were finally estimated as the ratio of these maximal growth rates to the number of coarse-grained resource pools used by each strain.

4.3.2 Calculation of intergenomic distances

To calculate intergenomic distances between members of the two synthetic gut communities [57, 58], we first identified reference genomes for each member from RefSeq using accession numbers listed in table S4 (for Ho et al.) or the corresponding publication [76] (for Weiss et al.). Genomic distances were then calculated between each species pair using GGDC 3.0 [77]. Reported values are based on the recommended formula 2, which returns the ratio between the number of dissimilar bases in high-scoring segment pairs (HSPs) and total HSP length.

5 Acknowledgements

We would like to thank Simon van Vliet, Prajwal Padmanabha and Eric Ulrich for their valuable comments on a previous version of this manuscript. We would also like to thank Vit Piskovsky, João Miranda, Ming Liu and Prajwal Padmanabha for useful discussions on linear stability, as well as Anna Weiss for OMM 12 community datasets. OJM was supported by a Human Frontier Science Program (HFSP) long-term fellowship (LT0020/2022-L) and a University of Sheffield Strategic Research Fellowship in the Physics of Life and Quantitative Biology. MA and SM were supported by the National Center of Competence in Research Microbiomes grant SNF 51NF40_180575, Swiss National Science Foundation (SNSF) Eccellenza grant PCEGP3_181272, and SNSF project grant 320030-236360.

6 Code availability statement

All code used to generate the results presented in this manuscript is available in https://github.com/Pseudomoaner/Kropotkin and https://github.com/Pseudomoaner/EOsimSuite.

7 Competing interests statement

The authors declare that they have no competing interests.

References

1. Bronstein, J. L. *Mutualism* en. Google-Books-ID: tlIdCgAAQBAJ. ISBN: 978-0-19-967566-1 (Oxford University Press, 2015).
2. Kost, C., Patil, K. R., Friedman, J., Garcia, S. L. & Ralser, M. Metabolic exchanges are ubiquitous in natural microbial communities. en. *Nature Microbiology* **8.** Publisher: Nature Publishing Group, 2244–2252. ISSN: 2058-5276. https://www.nature.com/articles/s41564-023-01511-x (2024) (Dec. 2023).
3. Bryant, M. P., Wolin, E. A., Wolin, M. J. & Wolfe, R. S. Methanobacillus omelianskii, a symbiotic association of two species of bacteria. en. *Archiv für Mikrobiologie* **59,** 20–31. ISSN: 1432-072X. https://doi.org/10.1007/BF00406313 (2026) (Mar. 1967).
4. Morris, B. E., Henneberger, R., Huber, H. & Moissl-Eichinger, C. Microbial syntrophy: interaction for the common good. *FEMS Microbiology Reviews* **37,** 384–406. ISSN: 0168-6445. https://doi.org/10.1111/1574-6976.12019 (2026) (May 2013).
5. Gregor, R. *et al.* Vitamin auxotrophies shape microbial community assembly on model marine particles. *The ISME Journal* **19,** wraf184. ISSN: 1751-7362. https://doi.org/10.1093/ismejo/wraf184 (2026) (Jan. 2025).
6. Yousif, G. *et al. Obligate cross-feeding of metabolites is common in soil microbial communities* en. Pages: 2025.01.29.635426 Section: New Results. Jan. 2025. https://www.biorxiv.org/content/10.1101/2025.01.29.635426v1 (2026).
7. Yu, J. S. *et al.* Microbial communities form rich extracellular metabolomes that foster metabolic interactions and promote drug tolerance. *Nature Microbiology* **7.** Publisher: Nature Publishing Group, 542–555. ISSN: 2058-5276. https://www.nature.com/articles/s41564-022-01072-5 (2023) (Mar. 2022).
8. Corral López, R. *et al.* Imbalance in gut microbial interactions as a marker of health and disease. *Science* **391.** Publisher: American Association for the Advancement of Science, 890–895. https://www.science.org/doi/full/10.1126/science.ady1729 (2026) (Feb. 2026).
9. Goldford, J. E. *et al.* Emergent simplicity in microbial community assembly. *Science* **361.** Publisher: American Association for the Advancement of Science, 469–474. ISSN: 10959203. http://science.sciencemag.org/ (2021) (Aug. 2018).
10. Gause, G. F. & Witt, A. A. Behavior of Mixed Populations and the Problem of Natural Selection. *The American Naturalist* **69.** Publisher: The University of Chicago Press, 596–609. ISSN: 0003-0147. https://www.journals.uchicago.edu/doi/abs/10.1086/280628 (2026) (Nov. 1935).
11. Coyte, K. Z., Schluter, J. & Foster, K. R. The ecology of the microbiome: Networks, competition, and stability. *Science* **350.** Publisher: American Association for the Advancement of Science, 663–666. ISSN: 10959203. https://www.science.org/doi/10.1126/science.aad2602 (2023) (Nov. 2015).
12. Allesina, S. & Tang, S. Stability criteria for complex ecosystems. *Nature* **483.** arXiv: 1105.2071 Publisher: Nature Publishing Group, 205–208. ISSN: 1476-4687. https://www.nature.com/articles/nature10832 (2022) (Feb. 2012).
13. Holland, J. N., Ness, J. H. & BRONSTEIN, J. L. Mutualisms as Consumer-Resource. *Ecology of predator-prey interactions.* Publisher: Oxford University Press, 17. https://books.google.com/books?hl=en&lr=&id=A4ORDAAAQBAJ&oi=fnd&pg=PA17&dq=info:ukF1bYyxCTsJ:scholar.google.com&ots=JfEI8xodZY&sig=TeTf8O68dP4-axdyujVtg3oYuxQ (2026) (2005).
14. Rohr, R. P., Saavedra, S. & Bascompte, J. On the structural stability of mutualistic systems. *Science* **345.** Publisher: American Association for the Advancement of Science, 1253497. https://www.science.org/doi/full/10.1126/science.1253497 (2026) (July 2014).
15. Jones, E. I., Bronstein, J. L. & Ferrière, R. The fundamental role of competition in the ecology and evolution of mutualisms. en. *Annals of the New York Academy of Sciences* **1256.**

_eprint: https://nyaspubs.onlinelibrary.wiley.com/doi/pdf/10.1111/j.1749-6632.2012.06552.x, 66–88. ISSN: 1749-6632. https://onlinelibrary.wiley.com/doi/abs/10.1111/j.1749-6632.2012.06552.x (2026) (2012).

16. Bastolla, U. *et al*. The architecture of mutualistic networks minimizes competition and increases biodiversity. en. *Nature* **458.** Publisher: Nature Publishing Group, 1018–1020. ISSN: 1476-4687. https://www.nature.com/articles/nature07950 (2026) (Apr. 2009).
17. Stone, L. The stability of mutualism. *Nature Communications* **11,** 2648. ISSN: 2041-1723. https://pmc.ncbi.nlm.nih.gov/articles/PMC7253468/ (2026) (May 2020).
18. Butler, S. & O'Dwyer, J. P. Cooperation and stability for complex systems in resource-limited environments. en. *Theoretical Ecology* **13,** 239–250. ISSN: 1874-1746. https://doi.org/10.1007/s12080-019-00447-5 (2026) (June 2020).
19. Wolin, C. L. & Lawlor, L. R. Models of Facultative Mutualism: Density Effects. *The American Naturalist* **124.** Publisher: The University of Chicago Press, 843–862. ISSN: 0003-0147. https://www.journals.uchicago.edu/doi/abs/10.1086/284320 (2026) (Dec. 1984).
20. Okuyama, T. & Holland, J. N. Network structural properties mediate the stability of mutualistic communities. en. *Ecology Letters* **11.** _eprint: https://onlinelibrary.wiley.com/doi/pdf/10.1111/j.1461-0248.2007.01137.x, 208–216. ISSN: 1461-0248. https://onlinelibrary.wiley.com/doi/abs/10.1111/j.1461-0248.2007.01137.x (2026) (2008).
21. Hale, K. R. S. & Valdovinos, F. S. Ecological theory of mutualism: Robust patterns of stability and thresholds in two-species population models. en. *Ecology and Evolution* **11.** _eprint: https://onlinelibrary.wiley.com/doi/pdf/10.1002/ece3.8453, 17651–17671. ISSN: 2045-7758. https://onlinelibrary.wiley.com/doi/abs/10.1002/ece3.8453 (2026) (2021).
22. Holland, J. N., DeAngelis, D. L. & Bronstein, J. L. Population Dynamics and Mutualism: Functional Responses of Benefits and Costs. *The American Naturalist* **159.** Publisher: The University of Chicago Press, 231–244. ISSN: 0003-0147. https://www.journals.uchicago.edu/doi/abs/10.1086/338510 (2026) (Mar. 2002).
23. Niehaus, L. *et al*. Microbial coexistence through chemical-mediated interactions. *Nature Communications* **10.** Publisher: Nature Publishing Group, 1–12. ISSN: 2041-1723. https://www.nature.com/articles/s41467-019-10062-x (2022) (May 2019).
24. Hoek, T. A. *et al*. Resource Availability Modulates the Cooperative and Competitive Nature of a Microbial Cross-Feeding Mutualism. *PLOS Biology* **14.** Publisher: Public Library of Science, e1002540. ISSN: 1545-7885. https://journals.plos.org/plosbiology/article?id=10.1371/journal.pbio.1002540 (2022) (Aug. 2016).
25. Johnson, C. A. & Bronstein, J. L. Coexistence and competitive exclusion in mutualism. en. *Ecology* **100.** _eprint: https://esajournals.onlinelibrary.wiley.com/doi/pdf/10.1002/ecy.2708, e02708. ISSN: 1939-9170. https://onlinelibrary.wiley.com/doi/abs/10.1002/ecy.2708 (2026) (2019).
26. MacArthur, R. Species packing, and what competition minimizes. *Proceedings of the National Academy of Sciences* **64.** Publisher: Proceedings of the National Academy of Sciences, 1369–1371. ISSN: 0027-8424. https://www.pnas.org/content/64/4/1369 (2021) (Dec. 1969).
27. O'Dwyer, J. P. Whence Lotka-Volterra?: Conservation laws and integrable systems in ecology. *Theoretical Ecology* **11.** Publisher: Springer Netherlands, 441–452. ISSN: 18741746. https://link.springer.com/article/10.1007/s12080-018-0377-0 (2022) (Dec. 2018).
28. Letten, A. D., Ke, P. J. & Fukami, T. Linking modern coexistence theory and contemporary niche theory. *Ecological Monographs* **87.** Publisher: John Wiley & Sons, Ltd, 161–177. ISSN: 1557-7015. https://onlinelibrary.wiley.com/doi/full/10.1002/ecm.1242 (2022) (May 2017).

29. Chesson, P. Mechanisms of Maintenance of Species Diversity. en. *Annual Review of Ecology, Evolution, and Systematics* **31.** Publisher: Annual Reviews, 343–366. ISSN: 1543-592X, 1545-2069. https://www.annualreviews.org/content/journals/10.1146/annurev.ecolsys.31.1.343 (2024) (Nov. 2000).
30. Koffel, T., Daufresne, T. & Klausmeier, C. A. From competition to facilitation and mutualism: a general theory of the niche. *Ecological Monographs* **91.** Publisher: John Wiley & Sons, Ltd, e01458. ISSN: 1557-7015. https://onlinelibrary.wiley.com/doi/full/10.1002/ecm.1458 (2023) (Aug. 2021).
31. Meszéna, G., Gyllenberg, M., Pásztor, L. & Metz, J. A. Competitive exclusion and limiting similarity: A unified theory. *Theoretical Population Biology* **69.** Publisher: Academic Press, 68–87. ISSN: 0040-5809. (2022) (Feb. 2006).
32. Momeni, B., Xie, L. & Shou, W. Lotka-Volterra pairwise modeling fails to capture diverse pairwise microbial interactions. *eLife* **6.** Publisher: eLife Sciences Publications Ltd. ISSN: 2050084X. (2022) (Mar. 2017).
33. Letten, A. D. & Stouffer, D. B. The mechanistic basis for higher-order interactions and non-additivity in competitive communities. *Ecology Letters* **22.** Publisher: John Wiley & Sons, Ltd, 423–436. ISSN: 1461-0248. https://onlinelibrary.wiley.com/doi/full/10.1111/ele.13211 (2023) (Mar. 2019).
34. Vet, S. *et al.* Bistability in a system of two species interacting through mutualism as well as competition: Chemostat vs. Lotka-Volterra equations. en. *PLOS ONE* **13.** Publisher: Public Library of Science, e0197462. ISSN: 1932-6203. https://journals.plos.org/plosone/article?id=10.1371/journal.pone.0197462 (2026) (June 2018).
35. Novak, M. *et al.* Characterizing Species Interactions to Understand Press Perturbations: What Is the Community Matrix? *Annual Review of Ecology, Evolution, and Systematics* **47.** Publisher: Annual Reviews Inc., 409–432. ISSN: 15452069. (2022) (Nov. 2016).
36. Tilman, D. Resources: A Graphical-Mechanistic Approach to Competition and Predation. *Source: The American Naturalist* **116,** 362–393. https://about.jstor.org/terms (2022) (1980).
37. Meacock, O. J. & Mitri, S. Environment-Organism Feedbacks Drive Changes in Ecological Interactions. en. *Ecology Letters* **28.** _eprint: https://onlinelibrary.wiley.com/doi/pdf/10.1111/ele.70027, e70027. ISSN: 1461-0248. https://onlinelibrary.wiley.com/doi/abs/10.1111/ele.70027 (2025) (2025).
38. Cui, W., Marsland, R. & Mehta, P. Les Houches Lectures on Community Ecology: From Niche Theory to Statistical Mechanics. *ArXiv,* arXiv:2403.05497v1. ISSN: 2331-8422. https://www.ncbi.nlm.nih.gov/pmc/articles/PMC10942479/ (2024) (Mar. 2024).
39. Picot, A., Shibasaki, S., Meacock, O. J. & Mitri, S. Microbial interactions in theory and practice: when are measurements compatible with models? en. *Current Opinion in Microbiology* **75,** 102354. ISSN: 1369-5274. https://www.sciencedirect.com/science/article/pii/S1369527423000917 (2023) (Oct. 2023).
40. Johnson, C. A. How mutualisms influence the coexistence of competing species. en. *Ecology* **102.** _eprint: https://esajournals.onlinelibrary.wiley.com/doi/pdf/10.1002/ecy.3346, e03346. ISSN: 1939-9170. https://onlinelibrary.wiley.com/doi/abs/10.1002/ecy.3346 (2026) (2021).
41. Clark, J. P. The Second Derivative and Population Modeling. en. *Ecology* **52.** _eprint: https://esajournals.onli 606–613. ISSN: 1939-9170. https://onlinelibrary.wiley.com/doi/abs/10.2307/1934148 (2025) (1971).
42. Ginzburg, L. R. The theory of population dynamics: I. Back to first principles. *Journal of Theoretical Biology* **122,** 385–399. ISSN: 0022-5193. https://www.sciencedirect.com/science/article/pii/S0022519386801801 (2025) (Oct. 1986).
43. Shou, W., Ram, S. & Vilar, J. M. G. Synthetic cooperation in engineered yeast populations. *Proceedings of the National Academy of Sciences* **104.** Publisher: Proceedings of the

National Academy of Sciences, 1877–1882. https://www.pnas.org/doi/abs/10.1073/pnas.0610575104 (2026) (Feb. 2007).
44. Dal Co, A., van Vliet, S., Kiviet, D. J., Schlegel, S. & Ackermann, M. Short-range interactions govern the dynamics and functions of microbial communities. *Nature Ecology and Evolution* **4.** Publisher: Nature Publishing Group, 366–375. ISSN: 2397-334X. https://www.nature.com/articles/s41559-019-1080-2 (2021) (Feb. 2020).
45. Müller, M. J. I., Neugeboren, B. I., Nelson, D. R. & Murray, A. W. Genetic drift opposes mutualism during spatial population expansion. *Proceedings of the National Academy of Sciences of the United States of America* **111.** Publisher: National Academy of Sciences ISBN: 0027-8424, 1037–1042. ISSN: 0027-8424. http://www.ncbi.nlm.nih.gov/pubmed/11087846 (2018) (Jan. 2014).
46. Hammarlund, S. P., Chacón, J. M. & Harcombe, W. R. A shared limiting resource leads to competitive exclusion in a cross-feeding system. en. *Environmental Microbiology* **21.** _eprint: https://enviromicro-journals.onlinelibrary.wiley.com/doi/pdf/10.1111/1462-2920.14493, 759–771. ISSN: 1462-2920. https://onlinelibrary.wiley.com/doi/abs/10.1111/1462-2920.14493 (2025) (2019).
47. Pignon, E., Holló, G., Steiner, T., van Vliet, S. & Schaerli, Y. Uptake and leakage rates differentially shape community arrangement and composition of microbial consortia. *The ISME Journal* **19,** wraf122. ISSN: 1751-7362. https://doi.org/10.1093/ismejo/wraf122 (2026) (Jan. 2025).
48. Ross, T. D., Im, H., Keogh, B. G., Klausmeier, C. A. & Venturelli, O. S. Metabolic interplay drives population cycles in a cross-feeding microbial community. en. *Nature Communications* **16.** Publisher: Nature Publishing Group, 8919. ISSN: 2041-1723. https://www.nature.com/articles/s41467-025-63986-y (2026) (Oct. 2025).
49. McDonald, J. A. K. *et al.* Evaluation of microbial community reproducibility, stability and composition in a human distal gut chemostat model. *Journal of Microbiological Methods* **95,** 167–174. ISSN: 0167-7012. https://www.sciencedirect.com/science/article/pii/S0167701213002716 (2026) (Nov. 2013).
50. Hernandez, M. J. Dynamics of transitions between population interactions: A nonlinear interaction □-function defined. *Proceedings of the Royal Society B: Biological Sciences* **265.** Publisher: Royal Society, 1433–1440. ISSN: 14712970. https://royalsocietypublishing.org/ (2023) (Aug. 1998).
51. Preussger, D., Giri, S., Muhsal, L. K., Oña, L. & Kost, C. Reciprocal Fitness Feedbacks Promote the Evolution of Mutualistic Cooperation. English. *Current Biology* **30.** Publisher: Elsevier, 3580–3590.e7. ISSN: 0960-9822. https://www.cell.com/current-biology/abstract/S0960-9822(20)30986-6 (2026) (Sept. 2020).
52. Mee, M. T., Collins, J. J., Church, G. M. & Wang, H. H. Syntrophic exchange in synthetic microbial communities. *Proceedings of the National Academy of Sciences* **111.** Publisher: Proceedings of the National Academy of Sciences, E2149–E2156. https://www.pnas.org/doi/abs/10.1073/pnas.1405641111 (2025) (May 2014).
53. Chesson, P. MacArthur's consumer-resource model. *Theoretical Population Biology* **37,** 26–38. ISSN: 0040-5809. https://www.sciencedirect.com/science/article/pii/004058099090025Q (2025) (Feb. 1990).
54. Saavedra, S. *et al.* A structural approach for understanding multispecies coexistence. en. *Ecological Monographs* **87.** _eprint: https://esajournals.onlinelibrary.wiley.com/doi/pdf/10.1002/ecm.1263, 470–486. ISSN: 1557-7015. https://onlinelibrary.wiley.com/doi/abs/10.1002/ecm.1263 (2025) (2017).
55. Spaak, J. W. & De Laender, F. Intuitive and broadly applicable definitions of niche and fitness differences. en. *Ecology Letters* **23.** _eprint: https://onlinelibrary.wiley.com/doi/pdf/10.1111/ele.13511, 1117–1128. ISSN: 1461-0248. https://onlinelibrary.wiley.com/doi/abs/10.1111/ele.13511 (2025) (2020).

56. Song, C., Barabás, G. & Saavedra, S. On the Consequences of the Interdependence of Stabilizing and Equalizing Mechanisms. *The American Naturalist* **194.** Publisher: The University of Chicago Press, 627–639. ISSN: 0003-0147. https://www.journals.uchicago.edu/doi/full/10.1086/705347 (2024) (Nov. 2019).
57. Ho, P.-Y., Nguyen, T. H., Sanchez, J. M., DeFelice, B. C. & Huang, K. C. Resource competition predicts assembly of gut bacterial communities in vitro. en. *Nature Microbiology* **9.** Publisher: Nature Publishing Group, 1036–1048. ISSN: 2058-5276. https://www.nature.com/articles/s41564-024-01625-w (2026) (Apr. 2024).
58. Weiss, A. S. *et al.* In vitro interaction network of a synthetic gut bacterial community. *The ISME Journal 2021 16:4* **16.** Publisher: Nature Publishing Group ISBN: 4139602101153, 1095–1109. ISSN: 1751-7370. https://www.nature.com/articles/s41396-021-01153-z (2023) (Dec. 2021).
59. Goldman, D. A. *et al.* Competition for shared resources increases dependence on initial population size during coalescence of gut microbial communities. *Proceedings of the National Academy of Sciences* **122.** Publisher: Proceedings of the National Academy of Sciences, e2322440122. https://www.pnas.org/doi/full/10.1073/pnas.2322440122 (2026) (Mar. 2025).
60. Orr, J. A., Armitage, D. W. & Letten, A. D. Coexistence Theory for Microbial Ecology, and Vice Versa. en. *Environmental Microbiology* **27.** Publisher: John Wiley & Sons, Ltd, e70072. ISSN: 1462-2920. https://enviromicro-journals.onlinelibrary.wiley.com/doi/10.1111/1462-2920.70072 (2026) (Mar. 2025).
61. May, R. M. Will a Large Complex System be Stable? en. *Nature* **238.** Number: 5364 Publisher: Nature Publishing Group, 413–414. ISSN: 1476-4687. https://www.nature.com/articles/238413a0 (2023) (Aug. 1972).
62. Godoy, O. *et al.* Cooperation maximizes biodiversity. en. *The American Naturalist*. https://www.journals.uchicago.edu/doi/10.1086/741536 (2026) (2026).
63. Drew, G. C., Stevens, E. J. & King, K. C. Microbial evolution and transitions along the parasite–mutualist continuum. en. *Nature Reviews Microbiology* **19.** Number: 10 Publisher: Nature Publishing Group, 623–638. ISSN: 1740-1534. https://www.nature.com/articles/s41579-021-00550-7 (2024) (Oct. 2021).
64. Palmer, J. D. & Foster, K. R. Bacterial species rarely work together. *Science* **376.** Publisher: American Association for the Advancement of Science, 581–582. ISSN: 10959203. https://www.science.org/doi/10.1126/science.abn5093 (2023) (May 2022).
65. Hammarlund, S. P., Gedeon, T., Carlson, R. P. & Harcombe, W. R. Limitation by a shared mutualist promotes coexistence of multiple competing partners. en. *Nature Communications* **12.** Publisher: Nature Publishing Group, 619. ISSN: 2041-1723. https://www.nature.com/articles/s41467-021-20922-0 (2026) (Jan. 2021).
66. Thompson, J. N. Variation in Interspecific Interactions. *Annual Review of Ecology and Systematics* **19.** Publisher: Annual Reviews, 65–87. ISSN: 0066-4162. https://www.jstor.org/stable/2097148 (2026) (1988).
67. Sakarchi, J. & Germain, R. M. MacArthur's Consumer-Resource Model: A Rosetta Stone for Competitive Interactions. *The American Naturalist* **205.** Publisher: The University of Chicago Press, 306–326. ISSN: 0003-0147. https://www.journals.uchicago.edu/doi/full/10.1086/733516 (2025) (Mar. 2025).
68. Pastore, A. I., Barabás, G., Bimler, M. D., Mayfield, M. M. & Miller, T. E. The evolution of niche overlap and competitive differences. en. *Nature Ecology & Evolution* **5.** Publisher: Nature Publishing Group, 330–337. ISSN: 2397-334X. https://www.nature.com/articles/s41559-020-01383-y (2026) (Mar. 2021).
69. Chesson, P. & Kuang, J. J. The interaction between predation and competition. en. *Nature* **456.** Publisher: Nature Publishing Group, 235–238. ISSN: 1476-4687. https://www.nature.com/articles/nature07248 (2025) (Nov. 2008).

70. Colyvan, M. & Ginzburg, L. R. The Galilean turn in population ecology. en. *Biology and Philosophy* **18,** 401–414. ISSN: 1572-8404. https://doi.org/10.1023/A:1024121002194 (2025) (June 2003).
71. Ciarmoli, B. & Marbach, S. *Recycling and complementary food sources hinder oscillatory dynamics in a microbial population* en. ISSN: 2692-8205 Pages: 2025.09.22.677798 Section: New Results. Sept. 2025. https://www.biorxiv.org/content/10.1101/2025.09.22.677798v1 (2026).
72. Yang, Y., Foster, K. R., Coyte, K. Z. & Li, A. Time delays modulate the stability of complex ecosystems. en. *Nature Ecology & Evolution* **7.** Publisher: Nature Publishing Group, 1610–1619. ISSN: 2397-334X. https://www.nature.com/articles/s41559-023-02158-x (2025) (Oct. 2023).
73. Van den Berg, N. I. *et al.* Ecological modelling approaches for predicting emergent properties in microbial communities. en. *Nature Ecology & Evolution* **6.** Publisher: Nature Publishing Group, 855–865. ISSN: 2397-334X. https://www.nature.com/articles/s41559-022-01746-7 (2025) (July 2022).
74. Sibly, R. M., Hone, J., Clutton-Brock, T. H., Sibly, R. M. & Hone, J. Population growth rate and its determinants: an overview. *Philosophical Transactions of the Royal Society of London. Series B: Biological Sciences* **357.** Publisher: Royal Society, 1153–1170. https://royalsocietypublishing.org/doi/abs/10.1098/rstb.2002.1117 (2025) (Sept. 2002).
75. Liu, X., Constable, G. W. A. & Pitchford, J. W. Feasibility and stability in large Lotka Volterra systems with interaction structure. *Physical Review E* **107.** Publisher: American Physical Society, 054301. https://link.aps.org/doi/10.1103/PhysRevE.107.054301 (2025) (May 2023).
76. Garzetti, D. *et al.* High-Quality Whole-Genome Sequences of the Oligo-Mouse-Microbiota Bacterial Community. *Genome Announcements* **5.** Publisher: American Society for Microbiology, 10.1128/genomea.00758–17. https://journals.asm.org/doi/10.1128/genomea.00758-17 (2026) (Oct. 2017).
77. Meier-Kolthoff, J. P., Carbasse, J. S., Peinado-Olarte, R. L. & Göker, M. TYGS and LPSN: a database tandem for fast and reliable genome-based classification and nomenclature of prokaryotes. *Nucleic Acids Research* **50,** D801–D807. ISSN: 0305-1048. https://doi.org/10.1093/nar/gkab902 (2026) (Jan. 2022).

Emergent competition resolves the paradox of stable microbial mutualisms – Supplementary Information

Oliver J. Meacock *[1,2], Massimo Amicone [2], and Sara Mitri [2]

[1]School of Biosciences, University of Sheffield, Sheffield, United Kingdom

[2]Department of Fundamental Microbiology, University of Lausanne, Lausanne, Switzerland

Contents

*o.meacock@sheffield.ac.uk

1 Supplementary Notes

1.1 Supplementary Note 1: Derivation of EO equations

To derive the accelerational EO (aEO) equation (Eq. 5), we find the temporal derivative of the PCGR of a focal species α in an EO system. Starting with our definition of the sensitivity function $g_\alpha(\boldsymbol{r})$ as the PCGR at $\boldsymbol{r}$ (Eq. 3), we obtain

$$\frac{d}{dt}\left(\frac{1}{x_\alpha}\frac{dx_\alpha}{dt}\right) = \frac{dg_\alpha(\boldsymbol{r})}{dt} \tag{S.1}$$

Applying the chain rule yields

$$\frac{d}{dt}\left(\frac{1}{x_\alpha}\frac{dx_\alpha}{dt}\right) = \nabla g_\alpha \cdot \frac{d\boldsymbol{r}}{dt}. \tag{S.2}$$

Next, we substitute the definition of the rate of environmental change (Eq. 2)

$$\frac{d}{dt}\left(\frac{1}{x_\alpha}\frac{dx_\alpha}{dt}\right) = \nabla g_\alpha \cdot \boldsymbol{\sigma} + \sum_\beta \nabla g_\alpha \cdot \boldsymbol{f}_\beta x_\beta. \tag{S.3}$$

Applying the definitions of the abiotic acceleration $\mu'_\alpha(\boldsymbol{r}) \equiv \boldsymbol{\sigma}(\boldsymbol{r}) \cdot \nabla g_\alpha(\boldsymbol{r})$ and the biotic acceleration $a'_{\alpha\beta}(\boldsymbol{r}) \equiv \nabla g_\alpha \cdot \boldsymbol{f}_\beta$ yields the aEO equation:

$$\frac{d}{dt}\left(\frac{1}{x_\alpha}\frac{dx_\alpha}{dt}\right) = \mu'_\alpha(\boldsymbol{r}) + \sum_\beta a'_{\alpha\beta}(\boldsymbol{r})x_\beta. \tag{S.4}$$

As noted in the main text, in an equilibrium environment $\frac{d}{dt}\left(\frac{1}{x_\alpha}\frac{dx_\alpha}{dt}\right) = 0$. Applying this assumption to the aEO equation results in the equilibrium Environment Organism (eEO) equation:

$$0 = \mu'_\alpha(\boldsymbol{r}^*) + \sum_\beta a'_{\alpha\beta}(\boldsymbol{r}^*)x_\beta, \tag{S.5}$$

In previous work [1], we derived two expressions which describe PCGRs in EO-type ecosystems under regimes in which the environment can change: the closed Environment-Organism (cEO) and fluctuating Environment-Organism (fEO) equations. While we previously derived these using a path integral approach, they can also be derived directly from the aEO equation. Integrating Eq. 5 yields the fEO equation

$$\frac{1}{x_\alpha}\frac{dx_\alpha}{dt} = g_\alpha(\boldsymbol{r}_0) + \int_0^t \mu'_\alpha(\boldsymbol{r}) \cdot d\tau + \sum_\beta \int_0^t a'_{\alpha\beta}(\boldsymbol{r})x_\beta \cdot d\tau. \tag{S.6}$$

This describes the current growth rate of α based on the history of its interactions with other species and allogenic processes, along with an initial growth rate $g_\alpha(\boldsymbol{r}_0)$. In closed systems $\mu'_\alpha = 0$, yielding the cEO equation:

$$\frac{1}{x_\alpha}\frac{dx_\alpha}{dt} = g_\alpha(\boldsymbol{r}_0) + \sum_\beta \int_0^t a'_{\alpha\beta}(\boldsymbol{r})x_\beta \cdot d\tau. \tag{S.7}$$

This family of equations represents different experimental scenarios. The cEO equation describes the dynamics of closed well-mixed systems (*e.g.* batch culture) and spatially structured systems under one dimensional flow (*e.g.* the lower gut) [1]. The fEO and aEO equations in turn describe open systems undergoing changes in environmental composition over time (*e.g.* seasonal variations in a lake), while the eEO equation captures open systems at equilibrium (*e.g.* a stable bioreactor). When a community with a given set of impacts and sensitivities is placed in these different contexts, we observe distinct but related dynamical outcomes. These equations allow us to formally relate these different outcomes to each other.

1.2 Supplementary Note 2: Comparison of separation of timescales and the accelerational mapping

Obtaining a general mapping between mechanistic theories and direct interaction models has been a long sought-after goal of theoretical ecology, as it would allow us to cast the interaction structure of ecosystems in terms of underlying biological mechanisms [2]. The standard way of approaching the problem is to assume a separation in the timescales of the environmental and population dynamics [3], as first introduced by MacArthur [4]. In brief, environmental variables are forced to equilibrate by setting Eq. 2 to zero, resulting in an algebraic constraint which can be substituted into Eq. 3. The construction of MacArthur's model ensures that the resulting composite coefficients can be mapped onto those of the gLV equation as constants.

While influential, this approach to the problem is brittle. Firstly, there is generally no natural separation between the two timescales, with environmental dynamics occurring at approximately the same rate as the population dynamics. Even more problematically for the study of systems fueled by abiotic resources, the mapping is not possible unless the environmental variables themselves have logistic dynamics (*i.e.* act as biotic resources with density-dependent reproduction rates) [2]. Separation of timescales is additionally used in other theoretical studies that do not assume logistic resource dynamics (*e.g.* [5]). However, the resulting models cannot be framed in terms of the gLV equation.

Our accelerational approach avoids these issues, providing a general and flexible mapping between the two frameworks. We can illustrate the differences between the two approaches by comparing the output of the EO mapping to MacArthur's original results. MacArthur's consumer-resource model can be written as:

$$\frac{1}{x_\alpha}\frac{dx_\alpha}{dt} = \left(\sum_\rho w_\rho p_{\rho\alpha} r_\rho\right) - m_\alpha, \tag{S.8a}$$

$$\frac{dr_\rho}{dt} = \frac{r_\rho \nu_\rho}{k_\rho}(k_\rho - r_\rho) - r_\rho \sum_\beta p_{\rho\beta} x_\beta, \tag{S.8b}$$

where k_ρ is the carrying capacity for biotic resource ρ, $p_{\rho\alpha}$ represents the rate at which ρ is consumed by species α and converted to its own biomass, w_ρ is the nutritional value of ρ, ν_ρ is the maximal rate of increase of ρ and m_α is α's mortality rate (note that terms representing biomass conversion efficiency have been set to unity to simplify the expressions while retaining the structure of the model).

Separation of timescales yields the phenomenological gLV parameters [4]

$$a_{\alpha\beta} = -\sum_\rho p_{\rho\alpha} p_{\rho\beta} w_\rho \frac{k_\rho}{\nu_\rho}, \tag{S.9a}$$

$$\mu_\alpha = \sum_\rho k_\rho w_\rho p_{\rho\alpha} - m_\alpha. \tag{S.9b}$$

To apply our timescale separation-free approach, we begin by writing equation S.9b in terms of impact, sensitivity and allogenic functions (Table S1). Application of the definitions of μ'_α and $a'_{\alpha\beta}$ yields

$$a'_{\alpha\beta} = -\sum_{\rho} p_{\rho\alpha} p_{\rho\beta} w_\rho r^*_\rho, \tag{S.10a}$$

$$\mu'_\alpha = \sum_{\rho} \frac{r^*_\rho \nu_\rho}{k_\rho} (k_\rho - r^*_\rho) w_\rho p_{\rho_\alpha}. \tag{S.10b}$$

As the PCGA-based parameterisation depends on the equilibrium environment $\boldsymbol{r}^*$, we must also identify this composition. In this case, this is given by the intersection of Zero Net Growth Isoclines (ZNGIs) where $g_\alpha = 0$ for all species [6, 7]. Assuming the number of resources is equal to the number of species, this occurs at $\boldsymbol{r}^* = \boldsymbol{m} M^{-1}$, where the elements of the matrix M are $M_{\rho\alpha} = w_\rho p_{\rho\alpha}$ and $\boldsymbol{m}$ is the vector of mortalities m_α.

Comparing the two results, we note that the units of $a_{\alpha\beta}$ and μ_α are $[\text{Time}]^{-1}[\text{Biomass}]^{-1}$ and $[\text{Time}]^{-1}$ respectively, while those of $a'_{\alpha\beta}$ and μ'_α are $[\text{Time}]^{-2}[\text{Biomass}]^{-1}$ and $[\text{Time}]^{-2}$. The additional unit of inverse time in the accelerational quantities corresponds to the timescale of the resource dynamics, which is no longer eliminated through separation of timescales.

We also observe that the definitions of both $a_{\alpha\beta}$ and $a'_{\alpha\beta}$ consist of the sum of the products of the consumption rates $p_{\rho\alpha}$ $p_{\rho\beta}$ with a factor that only depends on the resource index ($w_\rho \frac{k_\rho}{\nu_\rho}$ for $a_{\alpha\beta}$ and $w_\rho r^*_\rho$ for $a'_{\alpha\beta}$). In Chesson's analysis of MacArthur's model [8], the $w_\rho \frac{k_\rho}{\nu_\rho}$s become the weights in a weighted least-squares regression between $p_{\rho\alpha}$ and $p_{\rho\beta}$, with the square root of the resulting coefficient of determination R^2 then being proportional to the niche overlap (see also Supplementary Note 1.3.3). The similarities in the structure of the expressions for $a_{\alpha\beta}$ and $a'_{\alpha\beta}$ means that this argument also applies to the acceleration-based analysis of MacArthur's model, allowing us to relate niche overlap to the linear independence of the utilisation vectors $\boldsymbol{p}_\alpha$ and $\boldsymbol{p}_\beta$.

1.3 Supplementary Note 3: Equivalencies between rate-based and accelerational ecological frameworks

In the main text, we note that the eEO equation (Eq. S.5) is structurally equivalent to the gLV equation at equilibrium. In this Note, we discuss several concepts that can be translated between the two frameworks on the basis of this equivalence: carrying capacity, linear stability and the stabilising/equalising mechanisms of Modern Coexistence Theory (MCT).

1.3.1 Carrying capacity

In Lotka-Volterra type systems, the carrying capacity of a species K_α is defined as its equilibrium abundance in isolation:

$$\frac{1}{x_\alpha}\frac{dx_\alpha}{dt} = \mu_\alpha + a_{\alpha\alpha}x_\alpha \tag{S.11a}$$

$$\implies 0 = \mu_\alpha + a_{\alpha\alpha}K_\alpha \tag{S.11b}$$

$$\implies K_\alpha = -\frac{\mu_\alpha}{a_{\alpha\alpha}}. \tag{S.11c}$$

This captures the concept of self-limitation in ecosystems – assuming $a_{\alpha\alpha}$ is negative (due to self-competition) and μ_α is positive (*i.e* α can establish in the current environment in isolation), K_α is a positive, finite value that indicates the density of α at which competition with itself exactly balances its underlying ability to grow.

Similar logic can be applied to obtain an equivalent expression for our accelerational framework:

$$\frac{d}{dt}\left(\frac{1}{x_\alpha}\frac{dx_\alpha}{dt}\right) = \mu'_\alpha + a'_{\alpha\alpha}x_\alpha \tag{S.12a}$$

$$\implies 0 = \mu'_\alpha + a'_{\alpha\alpha}K_\alpha \tag{S.12b}$$

$$\implies K_\alpha = -\frac{\mu'_\alpha}{a'_{\alpha\alpha}} = -\frac{\nabla g_\alpha \cdot \boldsymbol{\sigma}}{\nabla g_\alpha \cdot \boldsymbol{f}_\alpha}. \tag{S.12c}$$

Though equivalent in structure, this equation gives us a deeper mechanistic understanding of self-limitation. For example, we can see that increasing the elements of $\boldsymbol{\sigma}$ representing input of beneficial environmental factors (for which $\nabla g_{\alpha\rho}$ is positive) and decreasing the input of harmful environmental factors (for which $\nabla g_{\alpha\rho}$ is negative) will generally increase the value of the numerator, raising the overall value of K_α. The denominator is a more complex structure, particularly as trade-offs may enforce correlations between the elements of the vectors ∇g_α and $\boldsymbol{f}_\alpha$. However, we may broadly expect that an increase in the uptake of beneficial factors and release of harmful factors by α will make the denominator more negative and so reduce the carrying capacity overall.

An interesting case arises when $\mu'_\alpha = 0$, as in closed ecosystems. While this superficially suggests that the carrying capacity is $K_\alpha = 0$, in many systems the intra-specific biotic acceleration $a'_{\alpha\alpha}$ is also equal to 0 at equilibrium. This may arise when the release of growth-promoting substrates is exactly balanced by their uptake, as for example during nutrient cycling by algae [9], or when impacts fall to zero, as at the end of a batch culture experiment once all nutrients have been depleted. Under these conditions the carrying capacity is no longer defined by Eq. S.12,

and is instead determined by the initial conditions of the system (*e.g.* the initial amount of available nutrients). This implies that we can obtain very limited information about underlying ecological processes from these steady-state abundances in closed systems [10].

1.3.2 Linear stability analysis

Linear stability analysis of dynamical systems proceeds by identifying equilibrium states of the system and finding the eigenvalues of the system's Jacobian matrix evaluated at those points. Eigenvalues with positive real part indicate that arbitrarily small perturbations from the equilibrium state will be amplified by internal dynamics, pushing the system away from that point and destabilising the system. For the gLV model, the equilibrium composition $\boldsymbol{x}^*$ is given by [11]

$$\boldsymbol{x}^* = -A^{-1}\boldsymbol{\mu}, \tag{S.13}$$

and the Jacobian J^* at this stationary point is given by

$$J^* = \begin{pmatrix} a_{11}\,x_1^* & a_{12}\,x_1^* & \dots & a_{1N}\,x_1^* \\ a_{21}\,x_2^* & a_{22}\,x_2^* & \dots & a_{2N}\,x_2^* \\ \vdots & \vdots & \ddots & \vdots \\ a_{N1}\,x_N^* & a_{N2}\,x_N^* & \dots & a_{NN}\,x_N^* \end{pmatrix} \tag{S.14}$$

$$= \mathrm{diag}(\boldsymbol{x}^*)A. \tag{S.15}$$

Performing equivalent analysis in mechanistic models proceeds by evaluating the Jacobian of the entire dynamical system, *i.e.* incorporating both population and environmental dynamics (*e.g.* [12], Appendix A of [13]). By concatenating our expressions for the population and environmental dynamics and assuming that all populations are at non-zero densities, we obtain

$$J^* = \left(\begin{array}{c|c} \frac{\partial}{\partial x_\beta}\left(\frac{dx_\alpha}{dt}\right) & \frac{\partial}{\partial r_\gamma}\left(\frac{dx_\alpha}{dt}\right) \\ \hline \frac{\partial}{\partial x_\beta}\left(\frac{dr_\rho}{dt}\right) & \frac{\partial}{\partial r_\gamma}\left(\frac{dr_\rho}{dt}\right) \end{array}\right) \text{ at } \boldsymbol{r}^*, \boldsymbol{x}^* \tag{S.16}$$

$$= \left(\begin{array}{c|c} 0 & \mathrm{diag}(\boldsymbol{x}^*)\nabla G \\ \hline F & \frac{\partial}{\partial r_\gamma}(\sigma_\rho + \sum_\beta \boldsymbol{f}_\beta\, x_\beta^*) \end{array}\right), \tag{S.17}$$

where F is a matrix consisting of all of the impact functions evaluated at $\boldsymbol{r}^*$, ∇G is the matrix of all sensitivity gradients evaluated at $\boldsymbol{r}^*$ and ρ and γ are indices for the environmental factors. We show the real part of the eigenvalues of this matrix for the two species and five species auxotrophy models in Figs. S4b and S6d, respectively.

To understand how this result relates to the gLV-based analysis, let us begin by assuming that the environmental dynamics do not depend on the values of the environmental factors within the neighbourhood of $\boldsymbol{r}^*$ (*i.e.* that $\frac{\partial}{\partial r_\gamma}(\sigma_\rho + \sum_\beta \boldsymbol{f}_\beta\, x_\beta^*) = 0$). This results in a 2×2 block matrix with blocks of zeros on the diagonal, for which the eigenvalues are given by $\pm\sqrt{\mathrm{eig}(\mathrm{diag}(\boldsymbol{x}^*)\nabla G F)} = \pm\sqrt{\mathrm{eig}(\mathrm{diag}(\boldsymbol{x}^*)A')}$. In other words, this simplifying assumption yields eigenvalues that are the square root of the eigenvalues s_k that we would obtain from a direct translation of Eq. S.15 from rate-based to accelerational quantities.

This result implies that combinations of A and $\boldsymbol{x}^*$ that produce at least one positive real eigenvalue in the gLV framework have corresponding A's and $\boldsymbol{x}^*$s in the simplified accelerational framework that have at least one positive real eigenvalue. This in turn implies that linear instability in the gLV framework corresponds to linear instability in the accelerational framework. Perhaps more surprisingly, combinations of A and $\boldsymbol{x}^*$ that produce only negative *real* eigenvalues (*i.e.* are stable gLV systems) have corresponding A's and $\boldsymbol{x}^*$s which produce paired *imaginary* eigenvalues. These correspond to neutrally stable systems, in which perturbations from the equilibrium state result in indefinite oscillations around that equilibrium.

Clearly the environmental self-regulation represented by $\frac{\partial}{\partial r_\gamma}(\sigma_\rho + \sum_\beta \boldsymbol{f}_\beta\, x^*_\beta)$ is playing an important role in ensuring convergence on the system's fixed point. Let us incorporate these terms into our analysis more carefully. Following [14], we can use Schur's formula to obtain the following defining equation for the full system's eigenvalues λ:

$$0 = \det(\lambda I_N)\det\left(\lambda I_M - \frac{\partial}{\partial r_\rho}(\sigma_\gamma + \sum_\beta \boldsymbol{f}_\beta\, x^*_\beta) - \frac{1}{\lambda}F\ \mathrm{diag}(\boldsymbol{x}^*)\nabla G\right), \tag{S.18}$$

where we denote the identity matrix of size N as I_N, N is the total number of populations and M is the total number of environmental factors. Assuming that the system is not neutrally stable ($\lambda \neq 0$), this becomes

$$0 = \det\left(\lambda I_M - \frac{\partial}{\partial r_\rho}(\sigma_\gamma + \sum_\beta \boldsymbol{f}_\beta\, x^*_\beta) - \frac{1}{\lambda}F\ \mathrm{diag}(\boldsymbol{x}^*)\nabla G\right). \tag{S.19}$$

It is difficult to make general statements about this equation. However, it is informative to consider the case of a chemostat in which only dilution at rate D contributes to the environmental self-regulation (*i.e.* $\nabla \boldsymbol{f}_\beta = 0$). As $\frac{\partial \sigma_\gamma}{\partial r_\rho} = -DI_M$ in this case, we obtain

$$0 = \det\left(\lambda I_M + DI_M - \frac{1}{\lambda}F\ \mathrm{diag}(\boldsymbol{x}^*)\nabla G\right) \tag{S.20a}$$

$$= \det\left(\lambda(\lambda + D)I_N - \mathrm{diag}(\boldsymbol{x}^*)A'\right), \tag{S.20b}$$

where we have used the Weinstein-Aronszajn identity in the final line. Referring to the eigenvalues of $\mathrm{diag}(\boldsymbol{x}^*)A'$ as s_k, we can write the eigenvalues λ_k of the dilution-only EO system as

$$\lambda_k(\lambda_k + D) = s_k, \tag{S.21}$$

with solution

$$\lambda_k = -\frac{D}{2} \pm \sqrt{\frac{D^2}{4} + s_k}. \tag{S.22}$$

The upshot of this analysis is that chemostat-type dilution of the environmental factors tends to stabilise the ecosystem. The term outside the square root ($-\frac{D}{2}$) is always real and negative, thus damps down the neutral oscillations that would result if the expression under the square root remained negative.

From these considerations, we can propose conditions for stability of Eq. S.17: firstly, the accelerational version of Eq. S.15 should have negative real eigenvalues to ensure neutral stability in the absence of environmental self-regulation. Secondly, environmental self-regulation should be dissipative (*e.g.* through environmental dilution) to dampen the resulting oscillations. Unfortunately, comparison of the eigenvalue spectra of the accelerational version of Eq. S.15 (Fig. S5a) and Eq. S.17 (Fig. S5b) for the two species amino acid production sweep shows this picture is overly simplistic. While the eigenvalues of the former are predominantly real and negative, we observe complex eigenvalues with negative real part and even positive real eigenvalues at the lowest production rates. Given that we observe stability in the full system, the environmental self-regulation must be doing more than merely damping neutral oscillations. Nonetheless, the similarity in the structure of the two sets of eigenvalues is striking and suggests that the eigenvalues of $\mathrm{diag}(\boldsymbol{x}^*)A'$ may be a good proxy for evaluating system stability under a broad range of contexts. Exploring the deeper connections between these two perspectives under a wider range of scenarios should be a focus of future work.

1.3.3 Modern Coexistence Theory

Modern Coexistence Theory (MCT) arose as an effort to consolidate coexistence mechanisms varying across scales and systems into a limited set of processes operating on similar mathematical principles [15, 16]. One of its most important conclusions is that influences on species coexistence can be mathematically partitioned into equalising mechanisms (processes that reduce the difference in average fitness between species) and stabilising mechanisms (processes that reduce the overlap of niches between species) [15]. We will focus on the two-species case here, noting in passing that the multi-species case can be investigated through other frameworks that may in principle be translated into our accelerational formulation through Eq. 6 [17].

Much of our understanding of MCT comes from two-species gLV systems. For competing species labelled 1 and 2, feasibility is determined by the solutions of the equations $x_1^* = \frac{a_{22}\mu_1 - a_{12}\mu_2}{a_{11}a_{22} - a_{21}a_{12}}$ and $x_2^* = \frac{a_{11}\mu_2 - a_{21}\mu_1}{a_{11}a_{22} - a_{21}a_{12}}$. Combining the feasibility requirements of both species implies that

$$\frac{a_{12}}{a_{22}} < \frac{\mu_1}{\mu_2} < \frac{a_{11}}{a_{21}} \tag{S.23}$$

must hold for mutual coexistence.

One of Chesson's insights was to show that the expression $\frac{a_{\alpha\beta}}{a_{\alpha\alpha}}$ also appears as the regression coefficient between the resource preference vectors in MacArthur's consumer-resource model (Supplementary Note 1.2, [8]), allowing this expression describing feasible coexistence to be formally related to the degree of similarity between the utilisation of resources by the two populations. This leads to a form of the feasibility criterion in which each component has been multiplied by $\sqrt{\frac{a_{22}a_{21}}{a_{11}a_{12}}}$:

$$\sqrt{\frac{a_{12}a_{21}}{a_{11}a_{22}}} < \frac{\mu_1}{\mu_2}\sqrt{\frac{a_{22}a_{21}}{a_{11}a_{12}}} < \sqrt{\frac{a_{11}a_{22}}{a_{12}a_{21}}}. \tag{S.24}$$

This expression states that the 'fitnesses ratio' $\frac{\mu_1}{\mu_2}\sqrt{\frac{a_{22}a_{21}}{a_{11}a_{12}}}$ must be between the 'niche overlap' $\sqrt{\frac{a_{12}a_{21}}{a_{11}a_{22}}}$ and its reciprocal for coexistence to be feasible. We must also account for stability, which is guaranteed if $a_{22}a_{11} > a_{21}a_{12}$. Thus, stable coexistence results provided both that Eq. S.24 holds and the niche overlap term $\sqrt{\frac{a_{12}a_{21}}{a_{11}a_{22}}}$ is less than 1. This latter condition is essentially

always met as self-limitation is stronger than partner suppression (*i.e.* a_{11} is more negative than a_{21} and a_{22} is more negative than a_{12}) under competition scenarios.

It should be emphasised that Eq. S.24 is not MCT in and of itself, but rather the result of applying MCT to the two-species gLV equation as a specific ecosystem model [16]. Alternative definitions of niche overlap and fitness differences have been proposed for more general models [17–19], although the compatibility of some of these alternative definitions with those of Eq. S.24 has been called into question [20].

The ability to write MacArthur's consumer-resource model in gLV form using separation of timescales (Section 1.2) has led to its widespread adoption as a basis for interpreting niche overlaps and fitness differences in mechanistic terms [7, 8, 20]. Our mapping between mechanistic models and the gLV equation (Eq. 6) allows us to generalise this approach for any mechanistic model by substituting in our effective gLV parameters evaluated at equilibrium:

$$\sqrt{\frac{a'_{12}a'_{21}}{a'_{11}a'_{22}}} < \frac{\mu'_1}{\mu'_2}\sqrt{\frac{a'_{22}a'_{21}}{a'_{11}a'_{12}}} < \sqrt{\frac{a'_{11}a'_{22}}{a'_{12}a'_{21}}}. \tag{S.25}$$

We discuss the application of this result to the two species auxotrophy model in the main text.

One downside of this formulation is that it loses its connection to the mutual invasibility criterion, which states that both species must be able to invade the other when inoculated at low density for them to stably coexist. This is because differing equilibrium environmental states may mean that the effective gLV parameters for a resident community with $N-1$ species are very different to those of the full N species community. However, the mutual invasibility criterion is known to have a number of deficiencies as a predictor of coexistence in mechanistic models [21]. In the case of our own model, it is impossible for either of the obligate mutualists to reach an equilibrium in the absence its partner (Fig. S1), meaning there is no such thing as a baseline single-species community which can be subjected to invasion. Our approach may provide further insights into the conditions under which the mutual invasibility criterion breaks down as a predictor of coexistence.

1.4 Supplementary Note 4: Competitive exclusion scenarios map to the coexistence boundary of two-species MCT

Application of MCT to two EO models through Eq. S.25 results in competitive exclusion falling on the boundary of the coexistence region (Figs. 4, S7). Here we prove that this is a general property of EO systems. Note that, as in the main text, all environmentally-dependent quantities ($\boldsymbol{\sigma}(\boldsymbol{r}^*)$, $g_\alpha(\boldsymbol{r}^*)$ etc.) are assumed to be evaluated at equilibrium and explicit dependence on $\boldsymbol{r}^*$ suppressed.

We begin by assuming that species 1 of a two-species EO system is able to competitively exclude the other. From equilibration of the environmental dynamics (Eq. 2) in the single-species case, we have:

$$\boldsymbol{\sigma} = -K_1 \boldsymbol{f}_1, \tag{S.26}$$

where K_1 is the carrying capacity of species 1 (Supplementary Note 1.3.1). Substituting the definition of this term into the above equation yields

$$\boldsymbol{\sigma} = \frac{\nabla g_1 \cdot \boldsymbol{\sigma}}{\nabla g_1 \cdot \boldsymbol{f}_1} \boldsymbol{f}_1. \tag{S.27}$$

Taking the scalar product of both sides with ∇g_2 and rearranging gives:

$$\frac{\nabla g_2 \cdot \boldsymbol{\sigma}}{\nabla g_1 \cdot \boldsymbol{\sigma}} = \frac{\nabla g_2 \cdot \boldsymbol{f}_1}{\nabla g_1 \cdot \boldsymbol{f}_1} \tag{S.28a}$$

$$= \frac{\mu_2'}{\mu_1'} = \frac{a_{21}'}{a_{11}'} \tag{S.28b}$$

When multiplied by $\sqrt{\frac{a_{11}' a_{12}'}{a_{22}' a_{21}'}}$, this equation defines the lower boundary of the coexistence region (Supplementary Note 1.3.3), proving our initial claim. A symmetrical argument can be applied to show that competitive exclusion by species 2 results in mapping of the ecosystem to the upper boundary of the coexistence region.

2 Supplementary Tables

Simulated system	Sensitivity functions	Impact functions	Allogenic function
Abiotic nutrient competition [5]	$g_\alpha = \sum_\rho b_\rho c_{\alpha\rho} m_\alpha(r_\rho) - \theta$	$f_{\alpha\rho} = -c_{\alpha\rho} m_\alpha(r_\rho)$	$\sigma_\rho = r_{\rho\ \mathrm{IN}} - d_\rho r_\rho$
	b_ρ = nutritional value of ρ, $c_{\alpha\rho}$ = consumption rate of ρ by α, d_ρ = degradation rate.		
Antibiotic-mediated coexistence [22]	$g_\alpha = m(r_4) e^{-b_\alpha r_\alpha} - \theta_\alpha$	$f_{\alpha\rho} = \begin{cases} c m_\alpha(r_4) & \text{if } \rho = \alpha+1 \ (\rho \text{ is secreted antibiotic}) \\ -d r_\rho & \text{if } \rho = \alpha+2 \ (\rho \text{ is degraded antibiotic}) \\ -m_\alpha(r_\rho) & \text{if } \rho = 4 \ (\rho \text{ is nutrient}) \\ 0 & \text{otherwise} \end{cases}$	$\boldsymbol{\sigma} = D(\boldsymbol{r}_{\mathrm{IN}} - \boldsymbol{r})$
	b_α = antibiotic toxicity, c = per-capita antibiotic production rate, d = antibiotic degradation rate.		
	$\boldsymbol{r}$: position α = α-targeting antibiotic, $\alpha+1$ = antibiotic secreted by α, $\alpha+2$ = antibiotic degraded by α, 4 = in-common nutrient.		
Nutrient cross-feeding [23]	$g_\alpha = \sum_\rho b_{\alpha\rho} c_{\alpha\rho} r_\rho - \theta_\alpha$	$f_{\alpha\rho} = -c_{\alpha\rho} r_\rho + \sum_\gamma d_{\alpha\rho\gamma} c_{\alpha\gamma} r_\gamma$	$\boldsymbol{\sigma} = D(\boldsymbol{r}_{\mathrm{IN}} - \boldsymbol{r})$
	$b_{\alpha\rho}$ = biomass conversion efficiency, $c_{\alpha\rho}$ = uptake rate of ρ by α, $d_{\alpha\rho\gamma}$ = stoichiometry matrix.		
Chemical-mediated interactions [24]	$g_\alpha = b_\alpha + \sum_\rho (m_\alpha^+(r_\rho) + c_{\alpha\rho}^- r_\rho)$	$f_{\alpha\rho} = d_{\alpha\rho} - o_{\alpha\rho} m_\alpha(r_\rho)$	$\boldsymbol{\sigma} = \mathbf{0}$
	$b_{\alpha\rho}$ = basal growth rate, $c_{\alpha\rho}$ = growth impact of ρ on α, $d_{\alpha\rho}$ = production rate of ρ by α, $o_{\alpha\rho}$ = yield constant.		
Tilman's consumer-resource model [6]	$g_\alpha = m_\alpha(\sum_\rho b_{\alpha\rho} r_\rho - c_\alpha) - D$	$f_{\alpha\rho} = -d_{\alpha\rho}$	$\boldsymbol{\sigma} = D(\boldsymbol{r}_{\mathrm{IN}} - \boldsymbol{r})$
	$b_{\alpha\rho}$ = value of ρ for α, c_α = energy allocated to α's maintenance, $d_{\alpha\rho}$ = consumption rate of ρ by α.		
MacArthur's consumer-resource model [4]	$g_\alpha = \sum_\rho b_\rho c_{\alpha\rho} r_\rho - \theta_\alpha$	$f_{\alpha\rho} = -c_{\alpha\rho} r_\rho$	$\sigma_\rho = \frac{r_\rho d_\rho}{o_\rho}(o_\rho - r_\rho)$
	b_ρ = nutritional value of ρ, $c_{\alpha\rho}$ = consumption rate of ρ by α, d_ρ = maximal reproduction rate of ρ, o_ρ = carrying capacity of ρ.		

Table S1: **Non-exhaustive list of established EO models.** b, c, d and o are model-specific parameters whose meanings are given below the model specification. $m_\alpha(r_\rho)$ denotes a Monod function acting on resource r_ρ with embedded half-velocity and maximal utilization rate constants. θ denotes a mortality rate, while D denotes a dilution rate. Superscripts $^+$ and $^-$ indicate that the associated terms only apply if they are positive or negative, respectively. ρ and γ are indices of the environment vector $\boldsymbol{r}$. Where necessary, the structure of the environment vector with respect to the species index α is also specified. Note that in some cases, indices in $\boldsymbol{r}$ are modulo the length of the environment vector (for example, index $\alpha+1$ in the antibiotic-mediated coexistence model is written fully as $(\alpha+1) \mod 3$). We suppress the modulo operation in these cases for notational compactness. Some additional constraints on parameters present in the original models (*e.g.* enforcing conservation of mass) are not specified. Please see cited publications for complete model specifications including parameter choices.

Parameter symbol	Parameter meaning	Value
$\nu_{\mathring{v}}$	Maximum growth rate of $\mathring{v}$	0.4
$\nu_{\mathring{w}}$	Maximum growth rate of $\mathring{w}$	0.4
$K_{\mathring{v}\ c}$	Half velocity constant for use of c by $\mathring{v}$	1.8
$K_{\mathring{v}\ v}$	Half velocity constant for use of v by $\mathring{v}$	0.8
$K_{\mathring{w}\ c}$	Half velocity constant for use of c by $\mathring{w}$	0.7
$K_{\mathring{w}\ w}$	Half velocity constant for use of w by $\mathring{w}$	1.4
$Y_{\mathring{v}\ c}$	Yield of $\mathring{v}$ from one unit of c	1
$Y_{\mathring{v}\ v}$	Yield of $\mathring{v}$ from one unit of v	5
$Y_{\mathring{w}\ c}$	Yield of $\mathring{w}$ from one unit of c	1
$Y_{\mathring{w}\ w}$	Yield of $\mathring{w}$ from one unit of w	10
ℓ_v	Production rate of v by $\mathring{w}$	0.025
ℓ_w	Production rate of w by $\mathring{v}$	0.05
$[c]_{\mathsf{IN}}$	Input concentration of carbon source	2
$[v]_{\mathsf{IN}}$	Input concentration of amino acid v	0
$[w]_{\mathsf{IN}}$	Input concentration of amino acid w	0

Table S2: **Parameters for the two-species auxotrophy model.** Note that values of ℓ_v, ℓ_w, $[v]_{\mathsf{IN}}$ and $[w]_{\mathsf{IN}}$ are modified in some figures. These modifications are specified in the figure caption or axes labels.

Parameter symbol	Parameter meaning	Value
$q_{\mathcal{Y}y}$	Consumption rate of y by $\mathcal{Y}$	1
$q_{\mathcal{Y}z}$	Consumption rate of z by $\mathcal{Y}$	0.5
$q_{\mathcal{Z}y}$	Consumption rate of y by $\mathcal{Z}$	0.35
$q_{\mathcal{Z}z}$	Consumption rate of z by $\mathcal{Z}$	1
D	Dilution rate	0.05

Table S3: **Parameters for the two-species substitutable resource cross-feeding model.** Note that values of $\phi_{\alpha\rho\gamma}$ are specified on the axes of Fig. S7

.

Species name	RefSeq accession number
Enterococcus hirae	GCF_016766815.1
Enterococcus faecalis	GCF_000393015.1
Enterococcus faecium	GCF_009734005.1
Escherichia fergusonii	GCF_020097475.1
Bacteroides thetaiotaomicron	GCF_014131755.1
Bacteroides fragilis	GCF_000025985.1
Bacteroides uniformis	GCF_044361425.1
Parabacteroides distasonis	GCF_018279895.1
Flavonifractor plautii	GCF_010508875.1
Clostridium scindens	GCF_004295125.1
Clostridium hylemonae	GCF_022845755.1
Clostridium symbiosum	GCF_040267475.1
Clostridium clostridioforme	GCF_012273195.1
Blautia producta	GCF_010669205.1
Clostridium hathewayi	GCF_025149285.1

Table S4: **Reference genomes used for intragenomic distance calculations of species described in Ho *et al.* [25].**

3 Supplementary Figures

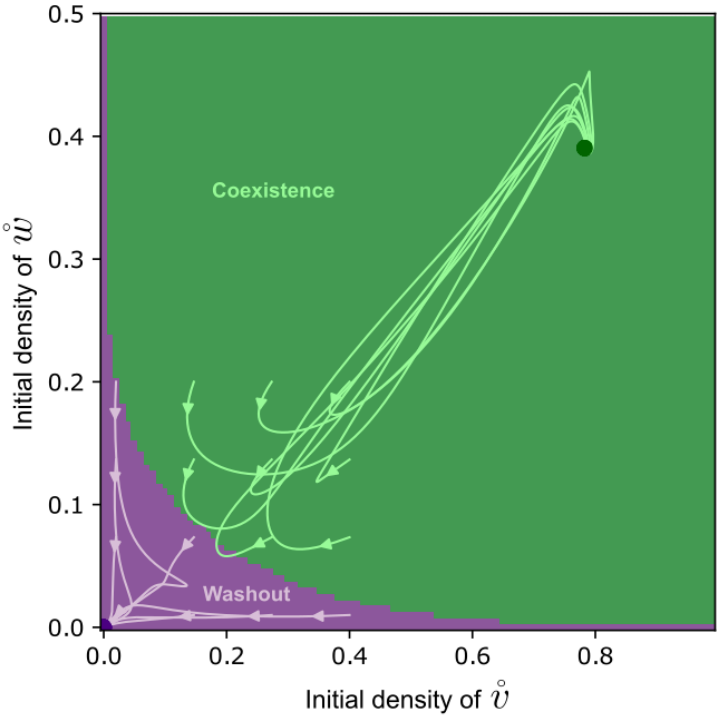

Figure S1: **Coexistence and Allee effects in the cross-feeding model.** Coloured sectors indicate basins of attraction for different starting densities for the two auxotrophs (green, mutual coexistence, purple, mutual extinction). Example trajectories converging on the two attractors (purple point and green point) are also shown. For a given starting density of one of the auxotrophs, pushing the starting density of the partner down to sufficiently low levels results in mutual extinction, an example of an Allee effect. This is a characteristic of obligate mutualisms [26]. Input media contains only the carbon source (no amino acids). $D = 0.01$.

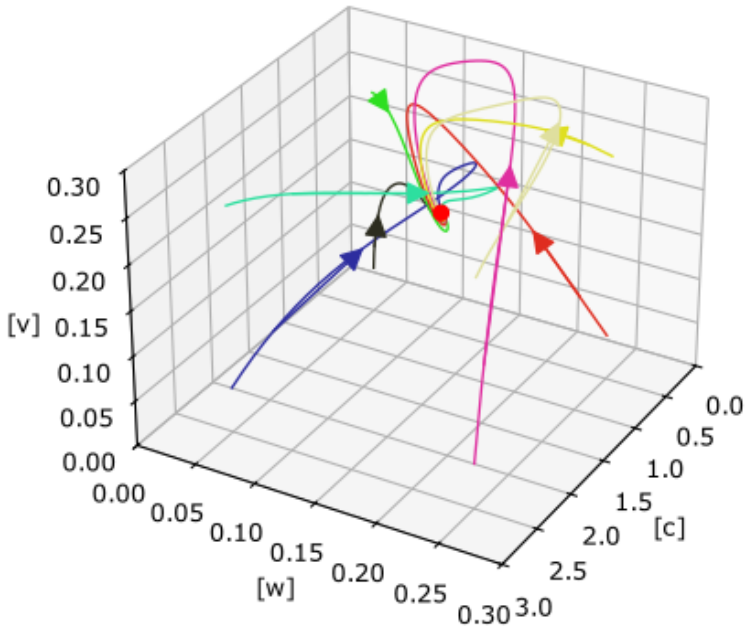

Figure S2: **The three-dimensional environment space.** Environmental trajectories for two-species chemostats initiated with varying initial compositions are plotted in different colours and converge on the equilibrium state $\boldsymbol{r}^*$ (red dot). Initial concentrations of the amino acids v and w are 0.05 or 0.25, while those of the carbon source c are 0.5 or 2.5. Input media contains only carbon at $[c]_{\text{IN}} = 3$. $D = 0.01$.

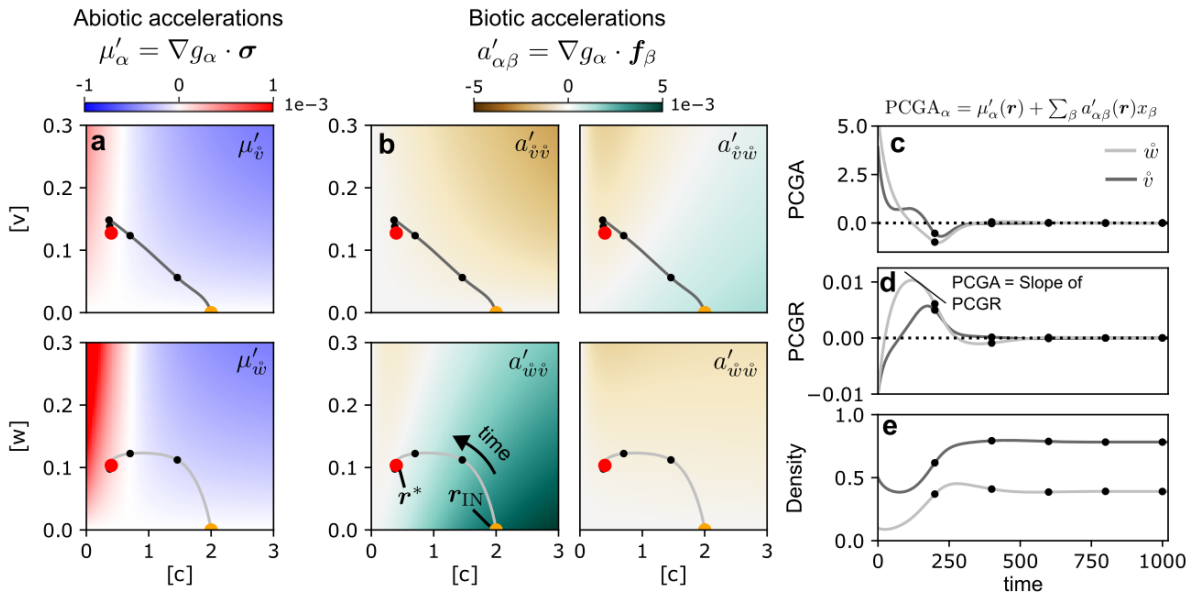

Figure S3: **The aEO equation describes ecosystem transients.** a,b) Scalar fields of the abiotic accelerations (a) and biotic accelerations (b), replicated from Fig. 2. We plot on top of these an environmental trajectory for a system initiated with the same environment as in the input media, which contains only carbon. The per-capita growth acceleration (PCGA) is determined by the aEO equation (Eq. 5), which is parameterised using the value of these scalar fields at each timepoint (c). Integration of the PCGA gives the time-varying per-capita growth rate (PCGR, d), which can itself be integrated to give the dynamics of the population densities (e). Black points along environmental trajectories (a,b) correspond to equally-spaced timepoints (c-e). $D = 0.01$.

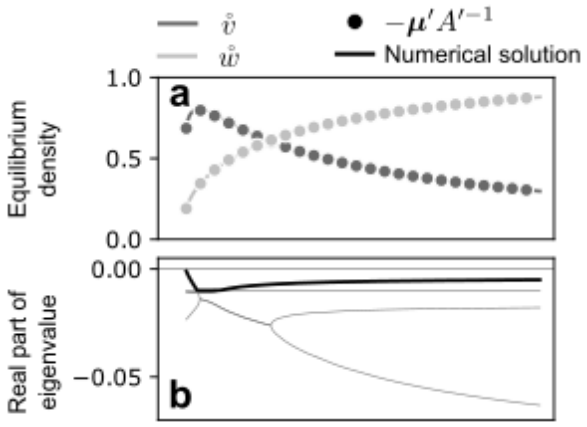

Figure S4: **Equilibrium abundances and stability analysis for amino acid production sweep.** Shown are equilibrium abundances (a) and the real part of the eigenvalue spectrum (b) (Supplementary Note 1.3.2, Fig. S5) for the set of simulations presented in Fig. 3. We also confirmed the equivalency between Eqs. 6 and 1 by using the values of the effective gLV parameters to estimate the equilibrium densities through the expression $\boldsymbol{\mu}' A'^{-1}$, where $\boldsymbol{\mu}'$ and A' are built from the equilibrium values shown in panels a and d of Fig. 3 (a, circles).

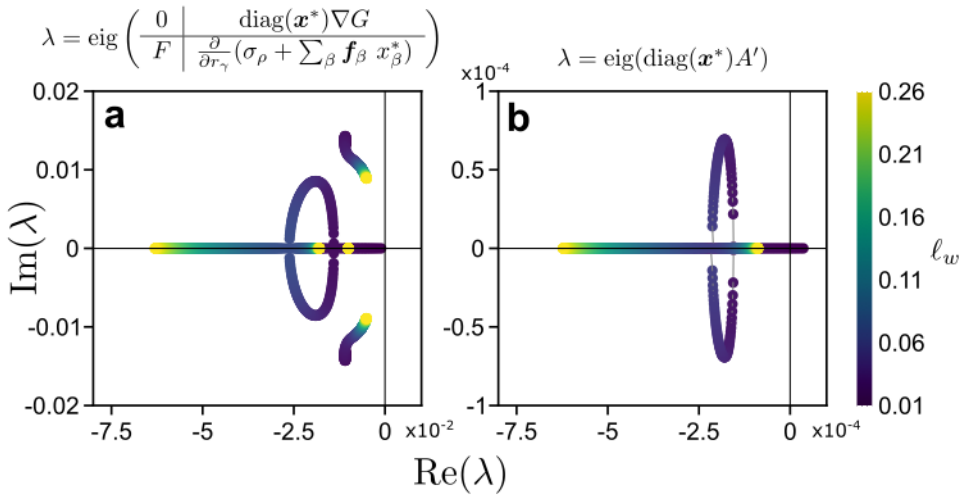

Figure S5: **Eigenvalue spectra for mechanistic models.** We show variations in the eigenvalue spectrum of the two-species auxotrophy model as the production rate of w by $\mathring{v}$ (ℓ_w) is varied. In a), we show the eigenvalues of the true Jacobian matrix which includes resource dynamics (Eq. S.17). In b), we show the eigenvalues of the matrix which is the accelerational analogue of the gLV Jacobian (Eq. S.15). The simulations used to construct this figure are the same as those used in Fig. 3. Note that we show the real part of panel a in Fig. S4b.

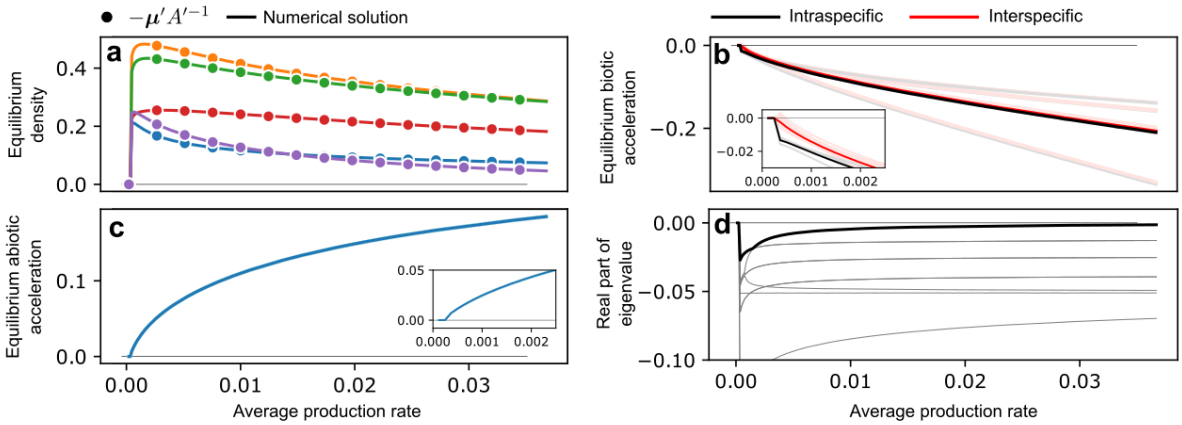

Figure S6: **5 species cross-feeding communities can be stable.** We constructed simulated communities of five auxotrophs with randomised mechanistic parameters and grew them in a chemostat on amino acid-free media (Methods). We show the equilibrium abundances (a), biotic accelerations (b, red lines indicate interspecific values and black lines intraspecific values), abiotic accelerations (c) and real part of eigenvalue spectrum (d) for different average amino acid production rates. Insets in panels b and c show zoomed-in regions of the main plot. Black line in d indicates value of the maximal eigenvalue.

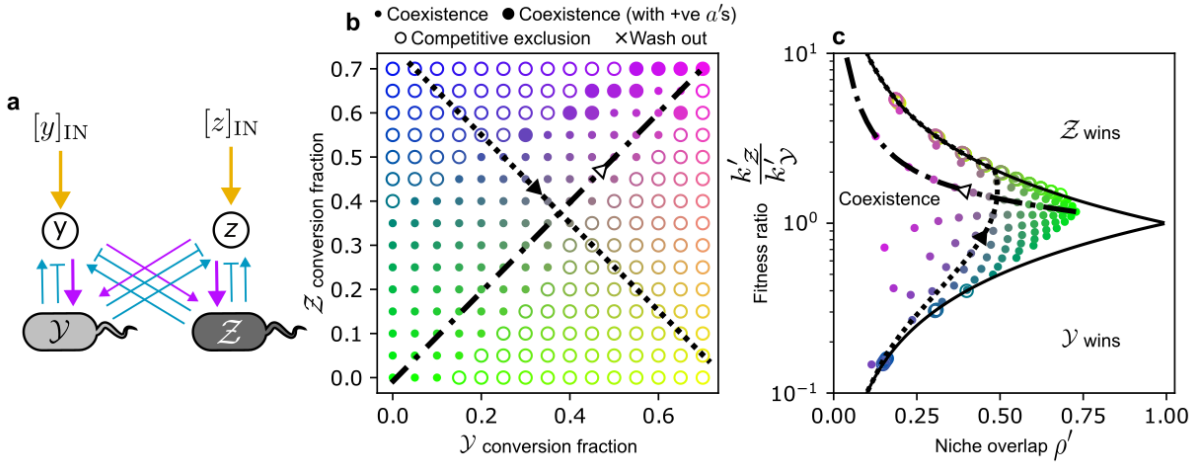

Figure S7: **Facultative cross-feeding of nutrients.** a) To test the importance of resource type in determining coexistence patterns in cross-feeding models, we implemented an EO model representing facultative cross-feeding of resources [23] (Methods). Two species $\mathcal{Y}$ and $\mathcal{Z}$ consume two carbon sources y and z with variable preferences; Y is specialised to consume y, while $\mathcal{Z}$ is specialised to consume z. A fraction of each consumed resource is then converted into the other type and secreted back into the environment. As both resources can be net consumed or produced by either species depending on their relative concentrations, we denote the impact functions (blue) as both positive and negative in the figure. b,c) We varied the fraction of consumed resource that was converted to the other type by each species and scored coexistence outcomes. Format of b, c is the same as in Fig. 4.

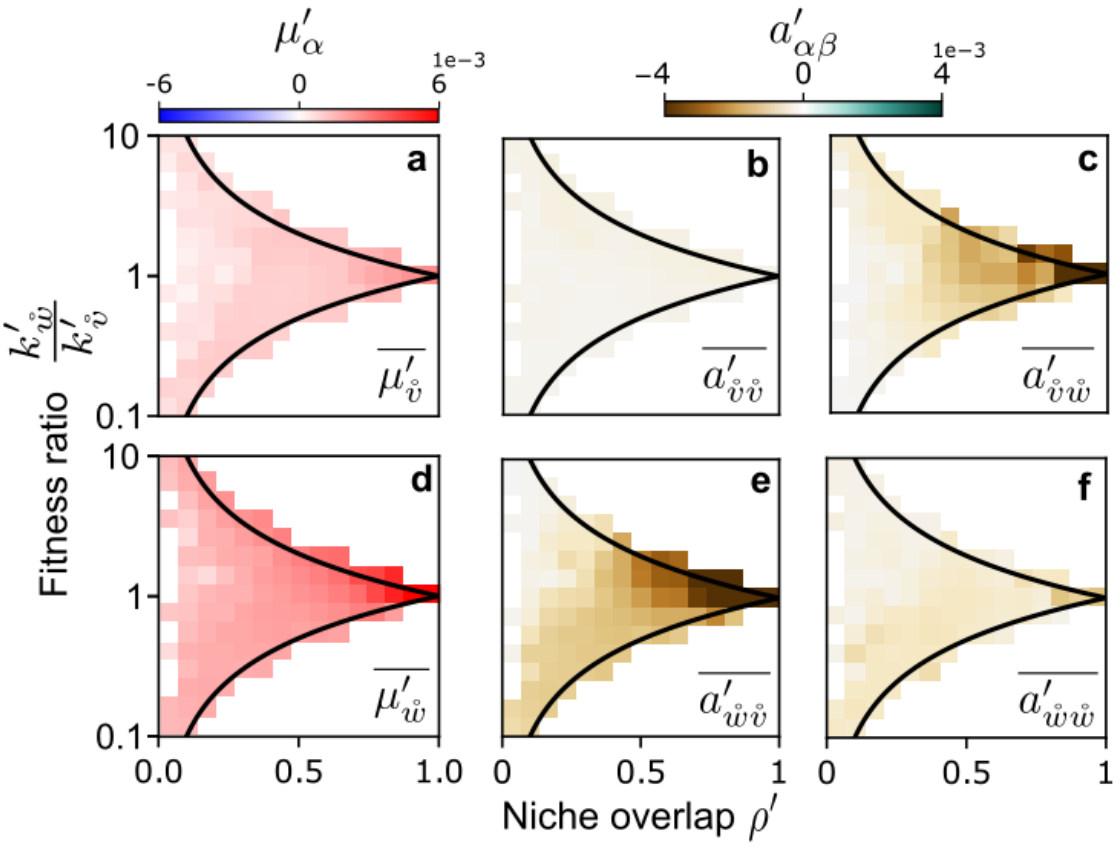

Figure S8: **Variation of effective gLV parameters on the niche overlap and relative fitness difference axes.** We display equivalent analysis as in Fig. 5a-g for the effective gLV parameters of the two species auxotrophy model. Shown are averages of abiotic accelerations (a,d) and biotic accelerations (b,c,e,f).

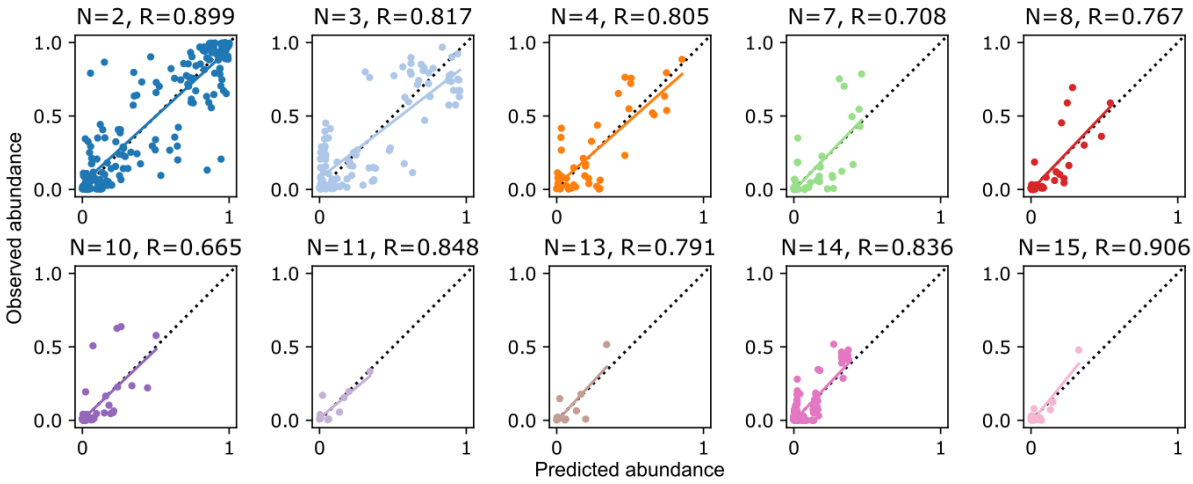

Figure S9: **Comparisons of coarse-grained EO model of Ho *et al.* [25] with competition experiments.** Each set of axes represents a group of competition experiments containing N species, indicated in the axis title along with the Pearson correlation coefficient R. The x-axis represents the equilibrium composition of the EO model initiated with the corresponding populations, while the y-axis represents the final abundances in the serial propagation experiment. All values are denoted as relative abundances. Dotted lines indicate unity.

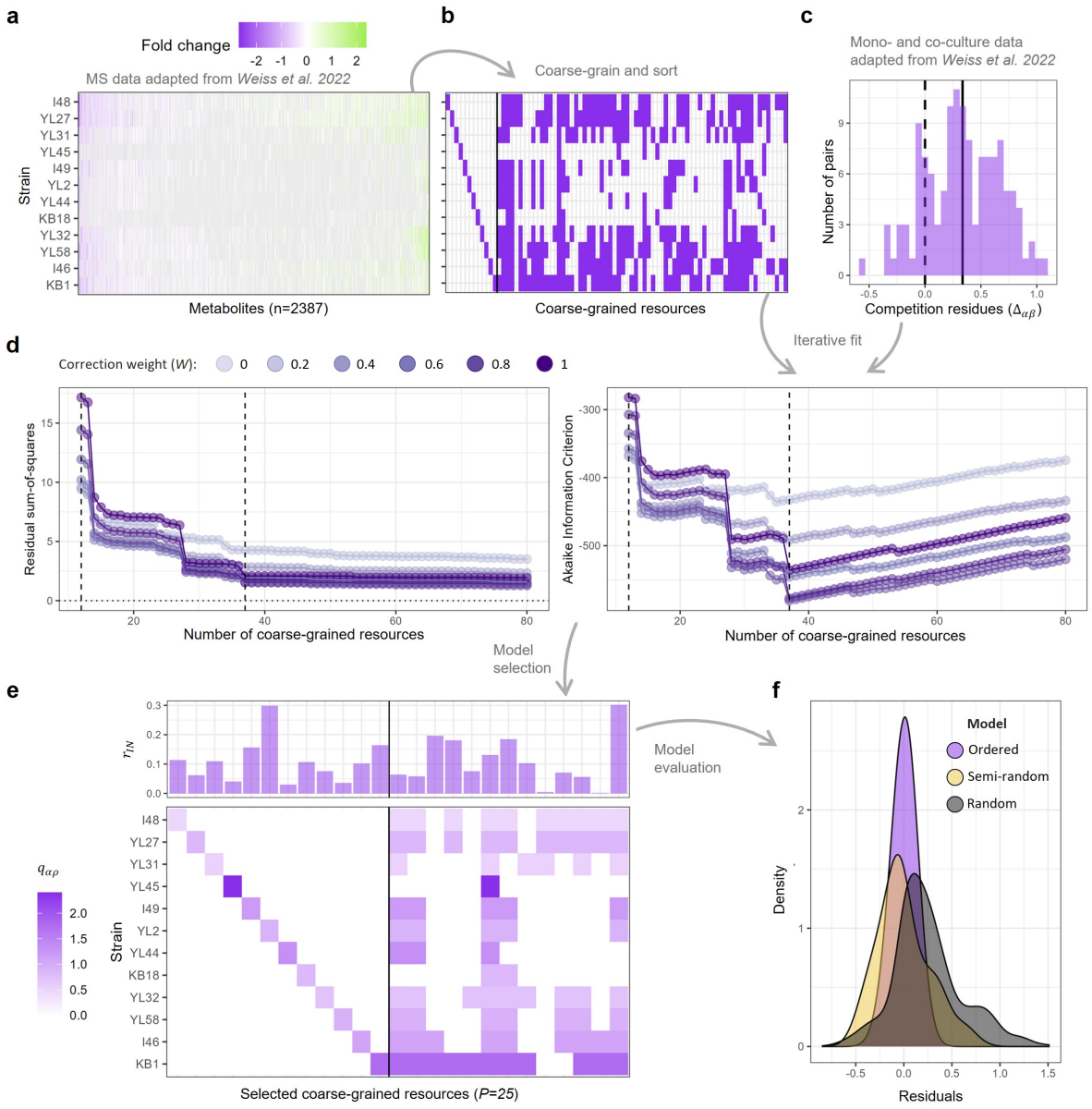

Figure S10: **Procedure for fitting coarse-grained consumer-resource model to OMM 12 data.** a) Relative enrichment of 2387 unidentified metabolites in spent media of each member of OMM 12 community compared to fresh media. Untargeted mass-spectrometry data (MS) adapted from Weiss *et al.* [27]. b) Consumption profile of each strain after coarse-graining and sorting of the depleted metabolite groups. c) Distribution of competition residues d) Goodness of fit to competition residues for all combinations of number of resource groups (P) and correction weight (W). The model with minimal Akaike Information Criterion is marked with the dashed vertical line and has correction weight $W = 0.6$ and $P = 37$ resource groups. e) Inferred parameters of the selected model. Only 25 coarse-grained resources out of 37 are shown as the remaining 12 had inferred input concentrations of zero. f) Comparison of residuals of predictions of spent and fresh media yields for the selected model ('Ordered') and two models with randomly selected coarse-grained resources. The 'Ordered' model uses the top 25 ranked resources for the fit; the 'Semi-random' model was fitted with the 12 unique resources plus 13 randomly selected coarse-grained resources; the 'Random' model used 25 randomly selected coarse-grained resources. Densities for each random model were estimated from 100 independent random samples.

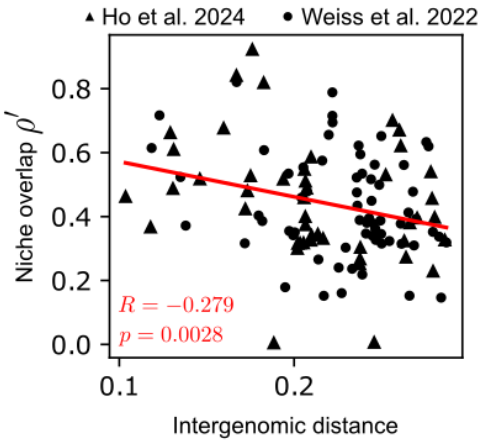

Figure S11: **Intergenomic distances correlate with niche overlaps.** To investigate the biological meaning of the accelerational interpretation of the niche overlap ρ', we compared the intergenomic distance between each species pair in the community of Ho *et al.* [25] and Weiss *et al.* [27] (Methods) with ρ' for that pair. The observed negative correlation was significant ($p = 0.0028$, linear regression t-test).

References

1. Meacock, O. J. & Mitri, S. Environment-Organism Feedbacks Drive Changes in Ecological Interactions. en. *Ecology Letters* **28.** _eprint: https://onlinelibrary.wiley.com/doi/pdf/10.1111/ele.70027, e70027. ISSN: 1461-0248. https://onlinelibrary.wiley.com/doi/abs/10.1111/ele.70027 (2025) (2025).
2. O'Dwyer, J. P. Whence Lotka-Volterra?: Conservation laws and integrable systems in ecology. *Theoretical Ecology* **11.** Publisher: Springer Netherlands, 441–452. ISSN: 18741746. https://link.springer.com/article/10.1007/s12080-018-0377-0 (2022) (Dec. 2018).
3. Sakarchi, J. & Germain, R. M. MacArthur's Consumer-Resource Model: A Rosetta Stone for Competitive Interactions. *The American Naturalist* **205.** Publisher: The University of Chicago Press, 306–326. ISSN: 0003-0147. https://www.journals.uchicago.edu/doi/full/10.1086/733516 (2025) (Mar. 2025).
4. MacArthur, R. Species packing, and what competition minimizes. *Proceedings of the National Academy of Sciences* **64.** Publisher: Proceedings of the National Academy of Sciences, 1369–1371. ISSN: 0027-8424. https://www.pnas.org/content/64/4/1369 (2021) (Dec. 1969).
5. Posfai, A., Taillefumier, T. & Wingreen, N. S. Metabolic Trade-Offs Promote Diversity in a Model Ecosystem. *Physical review letters* **118.** Publisher: NIH Public Access, 028103. ISSN: 10797114. /pmc/articles/PMC5743855/ (2022) (Jan. 2017).
6. Tilman, D. *Resource Competition and Community Structure*. ISBN: 978-0-691-08302-5. https://www.jstor.org/stable/j.ctvx5wb72 (2026) (Princeton University Press, 1982).
7. Letten, A. D., Ke, P. J. & Fukami, T. Linking modern coexistence theory and contemporary niche theory. *Ecological Monographs* **87.** Publisher: John Wiley & Sons, Ltd, 161–177. ISSN: 1557-7015. https://onlinelibrary.wiley.com/doi/full/10.1002/ecm.1242 (2022) (May 2017).
8. Chesson, P. MacArthur's consumer-resource model. *Theoretical Population Biology* **37,** 26–38. ISSN: 0040-5809. https://www.sciencedirect.com/science/article/pii/004058099090025Q (2025) (Feb. 1990).
9. De Jesús Astacio, L. M., Prabhakara, K. H., Li, Z., Mickalide, H. & Kuehn, S. Closed microbial communities self-organize to persistently cycle carbon. *Proceedings of the National Academy of Sciences* **118.** Publisher: Proceedings of the National Academy of Sciences, e2013564118. https://www.pnas.org/doi/abs/10.1073/pnas.2013564118 (2024) (Nov. 2021).
10. Dedrick, S., Warrier, V., Lemon, K. P. & Momeni, B. When does a Lotka-Volterra model represent microbial interactions? Insights from in vitro nasal bacterial communities. *mSystems* **8.** Publisher: American Society for Microbiology, e00757–22. https://journals.asm.org/doi/full/10.1128/msystems.00757-22 (2025) (June 2023).
11. Liu, X., Constable, G. W. A. & Pitchford, J. W. Feasibility and stability in large Lotka Volterra systems with interaction structure. *Physical Review E* **107.** Publisher: American Physical Society, 054301. https://link.aps.org/doi/10.1103/PhysRevE.107.054301 (2025) (May 2023).
12. Butler, S. & O'Dwyer, J. P. Stability criteria for complex microbial communities. *Nature Communications* **9.** Publisher: Nature Publishing Group, 1–10. ISSN: 2041-1723. https://www.nature.com/articles/s41467-018-05308-z (2022) (July 2018).
13. Liu, Y., Hu, J., Lee, H. & Gore, J. Complex Ecosystems Lose Stability When Resource Consumption Is Out of Niche. *Physical Review X* **15.** Publisher: American Physical Society, 011003. https://link.aps.org/doi/10.1103/PhysRevX.15.011003 (2026) (Jan. 2025).

14. Butler, S. & O'Dwyer, J. P. Cooperation and stability for complex systems in resource-limited environments. en. *Theoretical Ecology* **13,** 239–250. ISSN: 1874-1746. https://doi.org/10.1007/s12080-019-00447-5 (2026) (June 2020).
15. Chesson, P. Mechanisms of Maintenance of Species Diversity. en. *Annual Review of Ecology, Evolution, and Systematics* **31.** Publisher: Annual Reviews, 343–366. ISSN: 1543-592X, 1545-2069. https://www.annualreviews.org/content/journals/10.1146/annurev.ecolsys.31.1.343 (2024) (Nov. 2000).
16. Barabás, G., D'Andrea, R. & Stump, S. M. Chesson's coexistence theory. en. *Ecological Monographs* **88.** _eprint: https://esajournals.onlinelibrary.wiley.com/doi/pdf/10.1002/ecm.1302, 277–303. ISSN: 1557-7015. https://onlinelibrary.wiley.com/doi/abs/10.1002/ecm.1302 (2025) (2018).
17. Saavedra, S. *et al.* A structural approach for understanding multispecies coexistence. en. *Ecological Monographs* **87.** _eprint: https://esajournals.onlinelibrary.wiley.com/doi/pdf/10.1002/ecm.1263, 470–486. ISSN: 1557-7015. https://onlinelibrary.wiley.com/doi/abs/10.1002/ecm.1263 (2025) (2017).
18. Spaak, J. W. & De Laender, F. Intuitive and broadly applicable definitions of niche and fitness differences. en. *Ecology Letters* **23.** _eprint: https://onlinelibrary.wiley.com/doi/pdf/10.1111/ele.13511, 1117–1128. ISSN: 1461-0248. https://onlinelibrary.wiley.com/doi/abs/10.1111/ele.13511 (2025) (2020).
19. Koffel, T., Daufresne, T. & Klausmeier, C. A. From competition to facilitation and mutualism: a general theory of the niche. *Ecological Monographs* **91.** Publisher: John Wiley & Sons, Ltd, e01458. ISSN: 1557-7015. https://onlinelibrary.wiley.com/doi/full/10.1002/ecm.1458 (2023) (Aug. 2021).
20. Song, C., Barabás, G. & Saavedra, S. On the Consequences of the Interdependence of Stabilizing and Equalizing Mechanisms. *The American Naturalist* **194.** Publisher: The University of Chicago Press, 627–639. ISSN: 0003-0147. https://www.journals.uchicago.edu/doi/full/10.1086/705347 (2024) (Nov. 2019).
21. Orr, J. A., Armitage, D. W. & Letten, A. D. Coexistence Theory for Microbial Ecology, and Vice Versa. en. *Environmental Microbiology* **27.** Publisher: John Wiley & Sons, Ltd, e70072. ISSN: 1462-2920. https://enviromicro-journals.onlinelibrary.wiley.com/doi/10.1111/1462-2920.70072 (2026) (Mar. 2025).
22. Kelsic, E. D., Zhao, J., Vetsigian, K. & Kishony, R. Counteraction of antibiotic production and degradation stabilizes microbial communities. *Nature* **521.** Publisher: Nature Publishing Group, a division of Macmillan Publishers Limited. All Rights Reserved., 516–519. ISSN: 0028-0836. http://dx.doi.org/10.1038/nature14485 (2015) (May 2015).
23. Goldford, J. E. *et al.* Emergent simplicity in microbial community assembly. *Science* **361.** Publisher: American Association for the Advancement of Science, 469–474. ISSN: 10959203. http://science.sciencemag.org/ (2021) (Aug. 2018).
24. Niehaus, L. *et al.* Microbial coexistence through chemical-mediated interactions. *Nature Communications* **10.** Publisher: Nature Publishing Group, 1–12. ISSN: 2041-1723. https://www.nature.com/articles/s41467-019-10062-x (2022) (May 2019).
25. Ho, P.-Y., Nguyen, T. H., Sanchez, J. M., DeFelice, B. C. & Huang, K. C. Resource competition predicts assembly of gut bacterial communities in vitro. en. *Nature Microbiology* **9.** Publisher: Nature Publishing Group, 1036–1048. ISSN: 2058-5276. https://www.nature.com/articles/s41564-024-01625-w (2026) (Apr. 2024).
26. Hale, K. R. S. & Valdovinos, F. S. Ecological theory of mutualism: Robust patterns of stability and thresholds in two-species population models. en. *Ecology and Evolution* **11.** _eprint: https://onlinelibrary.wiley.com/doi/pdf/10.1002/ece3.8453, 17651–17671. ISSN: 2045-7758. https://onlinelibrary.wiley.com/doi/abs/10.1002/ece3.8453 (2026) (2021).
27. Weiss, A. S. *et al.* In vitro interaction network of a synthetic gut bacterial community. *The ISME Journal 2021 16:4* **16.** Publisher: Nature Publishing Group ISBN: 41396021011 53,

1095–1109. ISSN: 1751-7370. https://www.nature.com/articles/s41396-021-01153-z (2023) (Dec. 2021).